1987

Improved chromatographic detection methods based on absorbance and ultrasonic measurements

Kristen J. Skogerboe
Iowa State University

INFORMATION TO USERS

While the most advanced technology has been used to photograph and reproduce this manuscript, the quality of the reproduction is heavily dependent upon the quality of the material submitted. For example:

- Manuscript pages may have indistinct print. In such cases, the best available copy has been filmed.

- Manuscripts may not always be complete. In such cases, a note will indicate that it is not possible to obtain missing pages.

- Copyrighted material may have been removed from the manuscript. In such cases, a note will indicate the deletion.

Oversize materials (e.g., maps, drawings, and charts) are photographed by sectioning the original, beginning at the upper left-hand corner and continuing from left to right in equal sections with small overlaps. Each oversize page is also filmed as one exposure and is available, for an additional charge, as a standard 35mm slide or as a 17"x 23" black and white photographic print.

Most photographs reproduce acceptably on positive microfilm or microfiche but lack the clarity on xerographic copies made from the microfilm. For an additional charge, 35mm slides of 6"x 9" black and white photographic prints are available for any photographs or illustrations that cannot be reproduced satisfactorily by xerography.

Order Number 8721934

Improved chromatographic detection methods based on absorbance and ultrasonic measurements

Skogerboe, Kristen J., Ph.D.

Iowa State University, 1987

U·M·I
300 N. Zeeb Rd.
Ann Arbor, MI 48106

PLEASE NOTE:

In all cases this material has been filmed in the best possible way from the available copy. Problems encountered with this document have been identified here with a check mark __✓__.

1. Glossy photographs or pages _____
2. Colored illustrations, paper or print _____
3. Photographs with dark background _____
4. Illustrations are poor copy _____
5. Pages with black marks, not original copy _____
6. Print shows through as there is text on both sides of page _____
7. Indistinct, broken or small print on several pages ✓
8. Print exceeds margin requirements _____
9. Tightly bound copy with print lost in spine _____
10. Computer printout pages with indistinct print _____
11. Page(s) _____ lacking when material received, and not available from school or author.
12. Page(s) _____ seem to be missing in numbering only as text follows.
13. Two pages numbered _____. Text follows.
14. Curling and wrinkled pages _____
15. Dissertation contains pages with print at a slant, filmed as received _____
16. Other _____

_____

_____

University
Microfilms
International

Improved chromatographic detection methods based on absorbance and ultrasonic measurements

by

Kristen J. Skogerboe

A Dissertation Submitted to the
Graduate Faculty in Partial Fulfillment of the
Requirements for the Degree of

DOCTOR OF PHILOSOPHY

Department: Chemistry

Major: Analytical Chemistry

Approved:

Signature was redacted for privacy.

In Charge of Major Work

Signature was redacted for privacy.

For the Major Department

Signature was redacted for privacy.

For the Graduate College

Iowa State University
Ames, Iowa

1987

TABLE OF CONTENTS

CHAPTER 1.

OVERVIEW OF GAS AND LIQUID CHROMATOGRAPHY

Historical Development of Chromatography

The development of chromatography is one of the most important contributions to the advancement of science in this century. Today modern chromatography is the most widely used and powerful of all analytical separation techniques, and is in the forefront of developments in all areas of chemistry, biology, environmental science and medicine. The beauty of chromatography lies in its flexibility, relative simplicity and range of applications.

From its basic beginnings chromatography is a physical method for separating molecular species. The separation is based on the distribution of the species to be separated between two phases, one a stationary phase, the other a mobile phase that moves along the stationary phase. Such methods of phase distribution have not been restricted to modern implementation, as fixed beds of charcoal washed with water have for centuries been used to purify solutions (1). However, a formal report of this type of separation was not found in the scientific literature until 1834 when Runge reported the separation of plant extracts with paper as a stationary phase (2). In 1906 Tswett named the technique to describe the separation of chlorophylls using calcium carbonate as a stationary phase (3). Since most of the samples investigated in this study were pigments and dyes, the new method was called "chromatography," from the Greek words for "color" and "to write."

In the 80 years that have followed its official birth chromatography has gone through many cycles of rebirth and change. An explosion in application in 1940 occurred, beginning with the work of Martin and Synge (4). In 1952 Martin received a Nobel Prize for his work in chromatography. A complete review of chromatographic development has been undertaken by Ettre and Zlatkis (5).

Chromatography as a Separation Process

Chromatography is a single technique in a whole family of separation methods. Separation processes can be classified as either chemical, mechanical or physical. Table 1 gives examples of techniques which fit into these classes. The feature which distinguishes chromatography from other separation processes is that one phase is stationary while the other is mobile. This gives chromatography its enormous flexibility, because a wide variety of phases can be employed, and minute differences in the chemistry of components of a mixture can be exploited to achieve separations. Therefore, the stationary phase may be a solid, liquid, paper or gel, and the mobile phase can be either a liquid or gas. The two most commonly used types of chromatographic separation are gas-liquid chromatography (GC) and liquid chromatography (LC).

Table 1.

Separation Processes

Type	Examples
Chemical	Ion Exchange Precipitation Electrodeposition
Mechanical	Filtration Centrifugation
Physical	Chromatography Electrophoresis Extraction Distillation

GC Compared to LC

Because of its sensitivity, approximately 50% of all chromatographic analysis is done by GC. However, about 80% of the six million compounds listed in the chemical registry cannot be analyzed by GC because of volatility and thermal stability restrictions (6). Liquid chromatography is often a suitable alternate method for analysis of many of these compounds.

Improvements in column technology have largely been responsible for the current popularity of LC and GC. Development of chemically bonded stationary phases have represented a significant achievement in chromatography (7,8). Liquid chromatography methods that rely on these new stationary phases which can withstand higher pressures have been renamed high-performance liquid chromatography (HPLC). The general procedure to make these phases involves modification of silica, by a chemical reaction to produce a liquid stationary phase. The silica used in the reaction is often in one of two different forms. In one case, pelicular silica with diameters ranging from 5u to 20u is modified and used as the stationary phase in packed columns. Alternatively, the walls of a fused silica column are used as the reactive silica surface, to produce wall-coated open tubular columns. Until recently, open tubular columns have been used most extensively in GC; however, recent applications of columns of this type to LC have been reported (8-10).

There are many reactions which can be utilized to create a liquid stationary phase. A common reaction in column production converts

silanol (Si-OH) groups which are present on the surface of silica to alkyl silyl groups (11).

$$-SiOH + SOCl_2 \longrightarrow -SiCl$$

$$-SiCl + RMg \longrightarrow -SiR$$

The separation characteristics of the column can be widely varied by changing the alkyl group used in the reaction. A C_{18} alkyl group produces a non-polar stationary phase which will provide the most effective separation of non-polar analytes. When a polar mobile phase such as methanol or water is used the separation is called reverse phase chromatography (RPC). By contrast, normal phase chromatography refers to an LC system employing an unmodified silica stationary phase and a non-polar mobile phase. For either type of chromatography, even small changes in mobile phase composition can affect the retention and elution characteristics of analytes being separated.

Gas chromatographic separations are not classified in the same manner as those in LC because the gaseous mobile phases do not differ much in polarity. Helium, nitrogen, and hydrogen are the most commonly used carriers. Because these gases do not interact much with analytes, the stationary phase is primarily responsible for the separation. Changing the carrier gas doesn't change the elution order of analytes. For this reason GC separations are classified only by the polarity index of the stationary phase (12).

The development of open tubular capillary columns has represented a significant advancement in the area of GC. The

columns, formed from fused silica, have an inside diameter of between 0.05 and 0.5 mm. The absence of packing material causes the open tubular columns to have a small resistance to gas flow and therefore the columns can be as long as 100 meters without the presence of large backpressures. The advantage of long capillary columns is an enormous separatory power. A measure of this power, as determined by the ability of a column to separate components of a mixture, is the number of theoretical plates, N, which a column possesses. Commercially available capillary columns can often separate more than 100 different analytes present in a sample and have as many as 50,000 to 200,000 theoretical plates. This efficiency is at least 20 times better than that of larger diameter packed GC columns.

The separatory power of LC has traditionally been held as inferior to that of GC. The poorer efficiency is due to lower diffusivity of analytes in the liquid mobile phase. Typical ratios of the diffusion coefficient of an analyte in a gas to the same analyte in a liquid are on the order of 1×10^4 (13). The net result is that in LC mass transfer is very slow, and N values for typical packed columns may be 10 to 100 times less than for capillary GC columns. Improvements in LC efficiency have been made by using the open tubular columns, narrow-bore packed columns, or reducing the velocity of the mobile phase. Recently several microbore LC columns, each with 40,000 theoretical plates, have been coupled together to experimentally achieve one million theoretical plates (14). Even though this represents a remarkable accomplishment in LC, it took over 18 hours to

achieve a separation with such high efficiency. Therefore, the separatory power per unit time is still better for GC than for LC.

The trend toward smaller columns in both LC and GC has resulted in both improved efficiency and mass detectability. This advantage arises because the peak elution volumes are decreased because of the smaller column diameter. An additional benefit resulting from the use of these small-bore columns is reduced mobile phase consumption. Therefore, it is not cost prohibitive to use more expensive carrier gases and eluants because the flow rates are typically reduced from 1 ml/min to 50 ul/min for LC and from 30 ml/min to 1 ml/min for GC. The use of exotic mobile phases can result in increased selectivity in the separation and affords the applicability of a wide range of detection schemes.

The use of chiral eluants provides chromatographic resolution of enantiomeric amino acids (15). Microbore columns make the use of deuterated solvents feasible when nuclear magnetic resonance is used as an LC detector (16). Optically active mobile phases allow the spectropolarimeter, a highly selective detector of optical rotary dispersion, to be operated in an indirect mode, making it a universal detector (17). Finally, limited mobile phase consumption reduces the cost of argon when an ICP is used as a GC detector (18).

The use of microbore (and capillary) columns imparts important restrictions on the selection of a chromatographic detector. A general rule is that the detector volume should not be larger than the peak volume. If this requirement is not met, any advantage in

improved separation gained from the use of small-diameter columns may be negated due to peak broadening in the detector cell. This is especially important in LC, where peak volumes are smaller and most detectors respond on a concentration dependent mechanism. Microbore LC detectors should generally be no larger than 1 to 3 ul, above which peak broadening due to dead volume becomes important.

Chromatographic Detector Characteristics

Chromatographic detectors can be classified into two different types. Universal detectors give a signal for all analytes which pass through the detector cell, while selective detectors respond only to analytes which possess a certain property to which the detector is sensitive. Selective detectors are extremely useful in the analysis of complex mixtures where the column efficiency is not sufficient to separate each analyte. Universal detectors are useful when it is of interest to determine the number of components in a mixture, or the analytes do not exhibit any physical properties that could be conveniently exploited for selective detection. Finally, universal detection is useful when the structural nature of the sample is not known, so that selective detection cannot be applied.

The sensitivity of a detector, either selective or universal, is a primary consideration in the design of a chromatographic experiment. Whether a detector is classified as concentration or mass flow rate dependent determines to a large extent its sensitivity of response (19). The response of a concentration dependent detector decreases as

the volume of eluant eluted with the analyte increases. The response of mass flow dependent detectors is independent of the volume of carrier gas eluted with the sample. Absorbance, electron capture and refractive index detection are examples of detection in the concentration dependent mode. A well-known mass flow rate detector is the flame ionization detector (FID).

The trend toward small-bore columns can create a problem in detectability for concentration dependent detectors. The small volumes required for the detector cells often result in reduced detection pathlengths. For concentration mode detections such as absorbance and optical rotary dispersion, where sensitivity is directly related to pathlength, reduced volumes can lead to diminished sensitivity. Therefore, the challenge to make long path length, small-volume detectors, particularly in LC, is important.

The same challenges to develop small, sensitive LC detectors do not arise in GC, for two reasons. First, the peak volumes are relatively large, so that ultra-small cell volumes are not required. Second, optical detectors such as UV-absorbance are not commonly used in GC due to the lack of sensitivity and extreme selectivity of molecular absorbance in the gas phase. The one exception is fourier transform infra-red (FTIR), where the pathlength is increased by using a multiple reflection gold-lined cell called a lightpipe (20).

Two final important characteristics of chromatographic detectors are dynamic range and dynamic reserve. The former is defined as the ratio of the maximum and minimum detectable concentrations. In this

case, the maximum concentration is the concentration which causes a five-percent deviation from the predicted signal (19). For quantitation, a small dynamic range indicates that it is critical to verify that the detector signal is linear. Unless such a precaution is taken, the detector has poor quantitative reliability. Dynamic reserve (DR) is a measure of a detector's ability to measure a small signal on top of a large background signal. A detector with a large linear dynamic range does not necessarily have a large DR. This factor is much harder to measure, but refractive index and thermal conductivity detectors have a larger DR than ionization and absorbance based detectors. A large DR is an important parameter if a detector is to be used in an indirect detection mode (21,22). Indirect mode detection enables implementation of a unique quantitation scheme, where the concentration of an unidentified analyte can be determined without a calibration curve (23,24).

GC Detectors

The three GC detectors used most often are the thermal conductivity detector (TCD), Flame Ionization Detector (FID), and the Electron Capture Detector (ECD). Relevant properties of these and several other detectors are summarized in Table 2.

The universality, simplicity and reliability of the TCD make it the most widely used GC detector (19). However, since the TCD has only average sensitivity, the FID is rapidly growing in popularity because it is one-thousand-fold more sensitive. The FID is not a universal detector, as it will not respond to fixed gases, water and

Table 2.

Properties of GC Detectors

Detector	Response	Detectability	Typical Linear Range
TCD	Universal	10.0 ng	10^5
FID	Selective	10.0 pg	10^7
ECD	Selective	0.1 pg	10^4
Ultrasonic	Universal	1.0 pg	10^6
Gas Density	Selective	1.0 ng	10^3
FTIR	Selective	1.0 ng	10^3

some compounds which contain nitrogen and sulfur. In this detector, organic compounds are burned in an oxidative flame to produce ionized molecular fragments. The ions are collected at an electrode, creating a signal proportional to the number of ions formed. For organic analysis the FID is sensitive to virtually all analytes and is often assumed to be a universal detector.

The ECD is the most widely used selective detector. Since the ECD is selective for electronegative analytes, it has been used in the environmental analysis of halogenated polynuclear aromatic hydrocarbons (PAH) and pesticides (25). The ECD can detect halogenated analytes at the picogram level but will not respond to alkyl hydrocarbons unless an additive (such as O_2 or N_2O) is used to promote electron capture (26,27).

Liquid Chromatography Detectors

Detection in LC is generally less sensitive than that in GC. For the most part, sensitive GC detectors do not function well when the mobile phase is a liquid. The FID cannot be directly used as an LC detector due to the burden of the solvent on the flame. Developments in capillary LC have recently made FID-LC detection feasible, but superb detection limits have not yet been demonstrated (28).

Electron capture and thermal conductivity detection have been investigated in the liquid phase, but solvent association and other properties of liquids have so far rendered these detection schemes insensitive and difficult to understand (29,30). For example, the

work done in TC-LC detection indicates that the detector response is not simply a function of thermal conductivity, but also of heat capacity and molecular weight (30). Continued development of LC detectors based on the auxiliary properties such as TC, sound velocity, and magnetic susceptibility is an open field of research, with but a few contributions to the literature made each year (31,32).

The most popular LC detectors are refractive index (RI), absorbance, conductivity and fluorescence. Electrochemical detection is growing rapidly in popularity (33,34), as are hyphenated LC techniques based on FTIR (35,36) and mass spectrometric detection (37,38).

Just as GC detectors often do not work well in the liquid mode, the converse is true for LC detectors applied to GC. The RI detector, under the best conditions, can detect ng amounts of liquid analyte. However, in the gas phase only ug sensitivities are possible. Absorbance detection is improved in the condensed phase, due to broadened absorbance spectra, smaller peak volumes and concentration of the analyte so that sensitivity is improved. In the UV region, absorbance detection is only relatively selective because most aromatic organic molecules absorb in this region. However, sensitivity is still not impressive at the 0.1 ng level, even for molecules with large molar absorptivities (ε greater than 1000). For clinical and environmental analysis, mass detectability at even lower levels would aid in further understanding of such complex systems as brain function, viral disease and carcinogenic activity. In these

areas absorbance detection can be a more powerful analytical tool if the sensitivity can be increased to the picogram level or lower.

One LC detection mode which has achieved pg detectability is the fluorescence detector. One reason for the improved detectability is that the background contribution to the fluorescence signal is small. Furthermore, the fluorescence signal can be discriminated from background contributions such as stray light, Rayleigh and Raman scattering, and background fluorescence (39). Compared to an absorbance detector which responds only to molecules which absorb, the fluorometric detector responds only to molecules which first absorb and then fluoresce. Since relatively few molecules meet this requirement, fluorescence detection is highly selective, and has been used extensively to study PAHs. Since some members of this class of compounds are linked to carcinogenic activity, a highly selective and sensitive method for identifying their isomeric chemical structure is important in the areas of public health, medicine and toxicology (40-42).

Detector Summary

LC still does not equal GC in separation efficiency and detectability. In general, GC is often considered a mature science. On the other hand, many improvements in LC efficiency, detectability and selectivity are still required. A universal LC detector capable of picogram sensitivity in routine analysis situations needs to be developed. Capillary column development represents important research because of the need for improve chromatographic mass detectability.

But with their development come new challenges to create LC detectors with smaller cell volumes. The standard of detectability and separatory efficiency set by GC has opened a wide new area of analytical research with LC detection as the primary focus.

CHAPTER 2.

REAL TIME BACKGROUND-CORRECTED ABSORBANCE DETECTION IN MICROBORE LIQUID CHROMATOGRAPHY BASED ON A SINGLE FIBER OPTIC PROBE

A fast-growing and important area within analytical chemistry is the development of methods of analysis which are based on fiber optics. The popularity of optical fibers is due not only to their small diameter (5u - 2mm), but also to the long distances that these fibers will carry light without attenuation. This second characteristic has led to the implementation of optical fibers as signal carriers in long-distance telecommunications. While this application has received the most attention, the use of optical fibers in other areas is significant. The small diameter of the fiber makes possible new areas of in-vivo analysis (42) because they can be inserted into the body without damage to the tissue. In-vivo fiber probes have been developed to dynamically monitor pH, blood gases and glucose (43-45). The implication of these developments is that fiber probes can be utilized in operating and recovery rooms to continually monitor the analyte of interest. Not only can health care professionals obtain immediate laboratory results, but results such as pH and blood gas levels are not affected by sample exposure to air.

The low attenuation properties of fibers make them useful for remote sensing in environments where analysis is otherwise difficult. Long lengths of optical fiber enable light sources, monochrometers and detectors to be placed far from the site of analysis. Fiber optics

can be used for on-line monitoring of an industrial process (46), for the remote analysis of groundwater (47) or long-distance monitoring of radioactive materials (48).

Principles of Fiber Optic Probes

Optical fibers are usually made of a glass or silica core surrounded by a cladding. The refractive index of the core is always larger than the index of the cladding, so that the fiber traps light in the core due to total internal reflection (Figure 1).

If θ is the largest angle of incidence that allows light to be totally internally reflected, then Snell's Law applies,

$$n_o \sin \theta = n_1 \cos i_c \qquad (1)$$

where n_o is the refractive index of the originating medium and n_1 is the refractive index of the core.

The critical angle is then

$$\sin i_c = n_2/n_1 \qquad (2)$$

where the refractive index of the cladding is given by n_2. Therefore, light rays will be guided through the fiber only if angle i exceeds the critical angle.

The numerical aperture of an optical fiber is $n_o \sin \theta$, which is related to the refractive indices of the core and cladding.

$$n_o \sin \theta = (n_1^2 - n_2^2)^{1/2} \qquad (3)$$

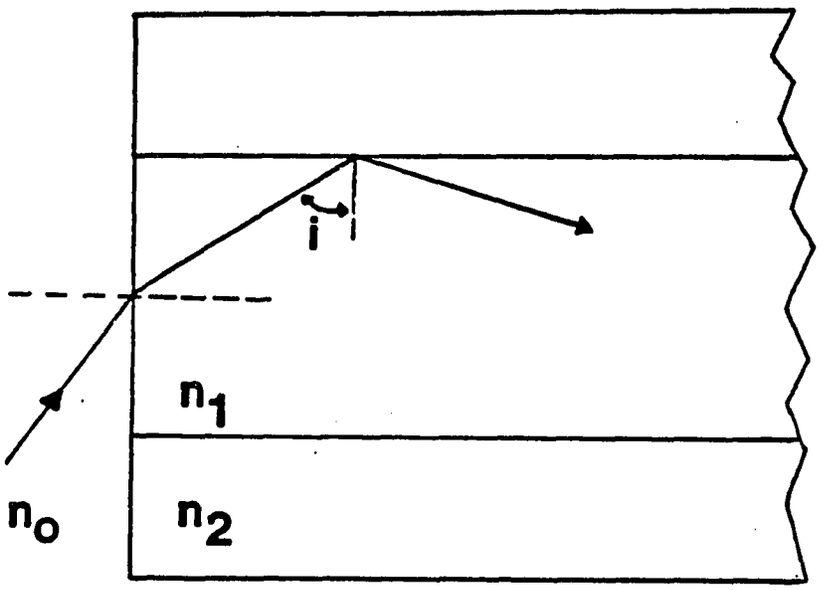

Figure 1. Transmission of light through an optical fiber n_o, refractive index of the originating medium; n_1, refractive index of the fiber core; n_2, refractive index of the fiber cladding; θ, greatest angle of incidence for total internal reflection, i, angle of reflection.

The numerical aperture, NA, is the maximum input angle at which light is guided. Then, for good efficiency in coupling light, the NA should not exceed that of the fiber.

After light is successfully coupled into an optical fiber its intensity can be attenuated due to three factors; Rayleigh scattering, absorption due to impurities and loss caused by bending the fiber (49). Small inhomogeneities in the fiber core causing scattering are primarily responsible for light attenuation. Since Rayleigh scattering is a function of $1/\lambda^4$, attenuation is greater at shorter wavelengths. Therefore, most fibers do not transmit well in the UV due to scattering as well as absorption.

Technology for making optical fibers is vastly improved, so that for longer wavelengths radiation lost to impurities is smaller compared to attenuation due to scattering. However, attenuation is readily increased if the fiber is bent or improperly handled. If it is of good quality and not wound too tightly, an average commercially available fiber will have an attenuation of about 3 dB/Km at 850 nm.

An important characteristic of fiber optics is the dispersion of a pulse of light propagating through the core. The dispersion, given in terms of the pulse broadening per kilometer of fiber, is important in applications utilizing modulation. Dispersion usually varies between one and twenty nanoseconds per kilometer, depending on the type of fiber employed.

Fiber optic probes

A number of fiber optic probes based on widely different principles have been developed (50). A considerable number of probes are fluorescence based where the fiber carries the excitation radiation to the sample. In fluorescence probes the emission is either measured directly from the analyte or is produced as a result of analyte-ligand interactions which promote fluorescence. In the latter case, immobilized ligands are coated onto the sampling end of the fiber optic, yielding a highly selective analytical probe. An example of a probe of this type involves immobilization of a dye onto the fiber surface. Specific interaction of the dye with various metal ions produces fluorescence (51). Other examples of probes based on fluorescence have been reported for measuring pH (43,52,53) and glucose (45).

Two other popular modes of detection in fiber probes are reflectance and absorbance. Reflectance based probes are sensitive to changes in the amount of reflected light at the fiber-sample interface. For uncoated fibers this is primarily a refractive index effect, as there is little penetration of the light into the sample. Probes for absorbance rely on a fixed pathlength for radiation passing through the sample.

Absorbance fiber probes

Optical fiber absorbance probes have been developed for in-vivo and remote sensing measurements. Several optical configurations are

possible (Figure 2), including one which uses two fibers: one to carry the radiation to the sample, the other to collect the unabsorbed light for detection. The advantages of a two-fiber system are the reduction of errors due to stray light and the provision of a well-defined pathlength. Unfortunately, such a bifurcated fiber system no less than doubles the diameter of the absorbance probe. So that the probe is not destructive, two-fiber probes are not suited for in-vivo medical applications because the size of the probe necessarily needs to be small.

A 600u diameter in-vivo fiber probe based on a single fiber has been developed (54). The probe was designed to produce a set pathlength by using a small mirror inside the needle which guides the fiber into the body. A large negative deviation from Beer's law is observed due to stray light present in the probe. The absorbance signal can be corrected for stray light by subtracting the background signal of a highly absorbing analyte from the sample absorbance (55). This approach is useful but is limited, for several reasons. The background correction decreases the precision of the absorbance measurement due to propagation of error through the subtraction. Also, changes in local environment, such as refractive index, are reflected in the amount of stray light; therefore, background correction is not complete. Finally, it is not well suited for on-line analysis, unless the correction is made simultaneously.

The development of a new absorbance fiber probe is described in

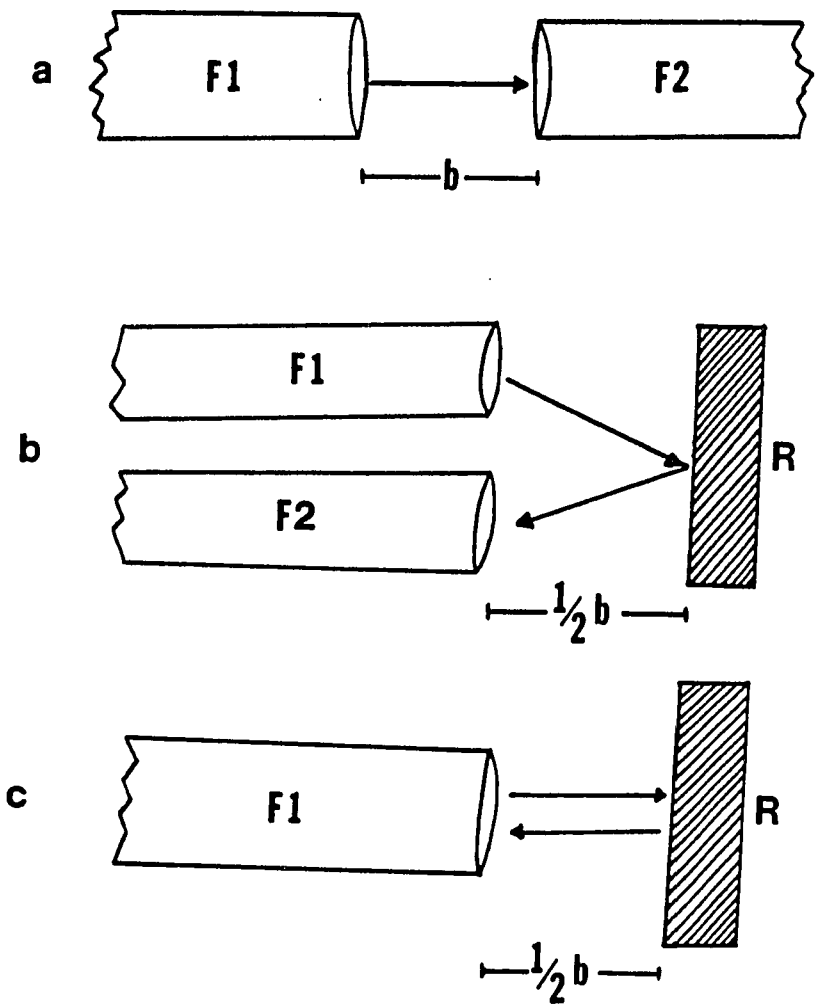

Figure 2. Configurations for fiber optic absorbance probes F1 and F2 are optical fibers; R, reflecting surface; b, pathlength; a) linear two-fiber probe; b) bifurcated parallel probe; c) single-fiber probe.

the remainder of this chapter. This spectrophotometric probe measures real-time absolute absorbance by minimizing the stray light contribution to the signal. This is accomplished via a coupling cell which matches the refractive index of the optical fiber to minimize reflections and an optical delay line based on high-frequency modulation to further reduce stray light. The probe utilizes a very small 140u-diameter optical fiber so that insertion of the probe is relatively non-invasive.

An interesting application of the probe is as a detector for microbore HPLC. We demonstrate that by inserting the probe parallel to eluant flow directly at the end of a microbore chromatography column, a pathlength of 3 mm can be obtained with a minimum cell volume of only 0.049 ul. Previously, absorbance cells for microbore separations have either been an on-column type with light passing through the sample perpendicular to eluant flow, or a Z-type, which allows light to propagate parallel to eluant flow (Figure 3 a-b). The on-column type detectors provide extremely small cell volumes but limit the pathlength to the width of the column inside diameter (56-57). The Z-type detector provides a longer optical path, but introduces band broadening, since the eluant must flow around two right-angle corners. We demonstrate that inserting the fiber probe parallel to the eluant flow provides on-column detection without sacrificing pathlength (Figure 3c).

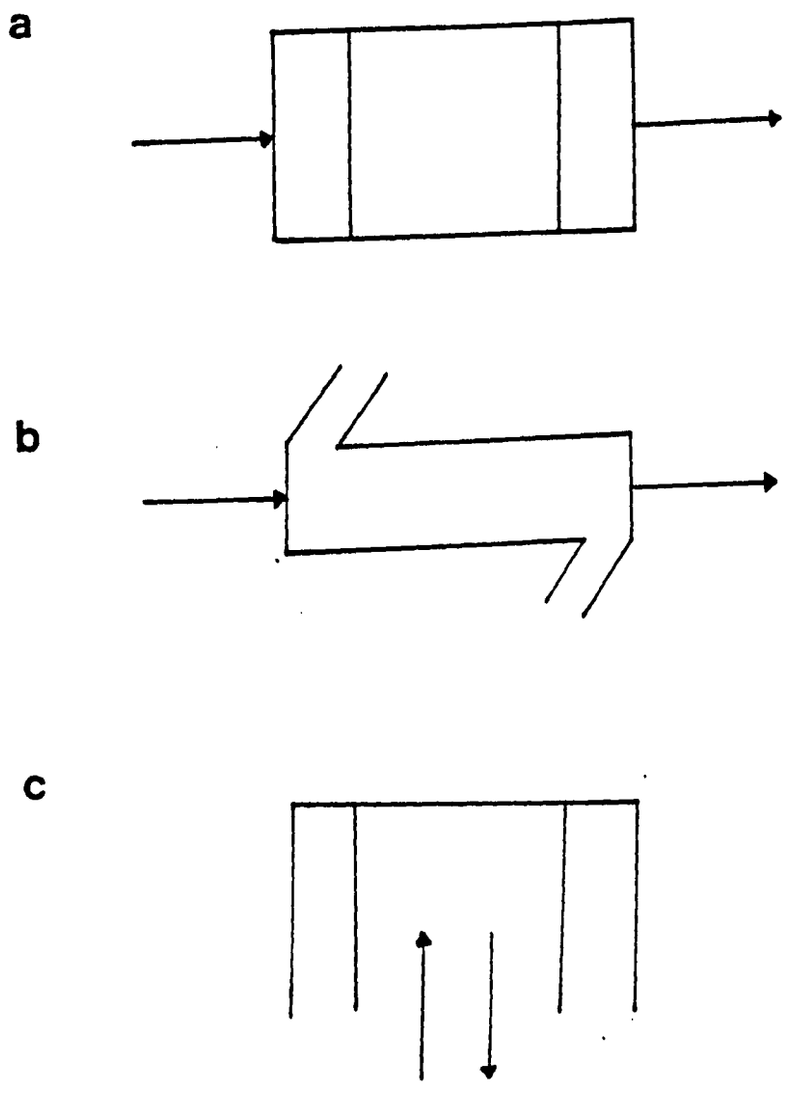

Figure 3. Absorbance cell configurations
a) on-column detection perpendicular to eluant flow, b) Z-type detection, c) on-column detection parallel to eluant flow.

Theory

Stray light is defined as light which is detected but has not passed through the sample (55). In a conventional absorbance detector, stray light can be reduced to less than 0.1% by careful instrument design. For a fiber-based absorbance detector it is employ a single fiber arrangement. One source of spurious radiation comes from light reflected at the fiber interface as light is focused into the fiber. For any interface a difference in refractive index causes scattered light. The amount of reflected light at an interface can be calculated by

$$\rho = \frac{(n_2 - n_1)^2}{(n_2 + n_1)^2} \qquad (4)$$

ρ is the percentage of light reflected and n_1 and n_2 are the refractive indices of the two mediums through which light is passing (58). For a single fiber probe there are two interfaces which can contribute stray light to the signal. Figure 4 identifies these as the coupling and absorbance cell interfaces. For the coupling interface, where light is focused into the optical fiber from air, reflected light is 4% of the total intensity. This reflected light, if detected, would represent a significant amount of stray light. This amount can be reduced if the medium carrying light to the fiber is changed from air to a medium with a higher refractive index. By matching the refractive index of the coupling medium to that of the

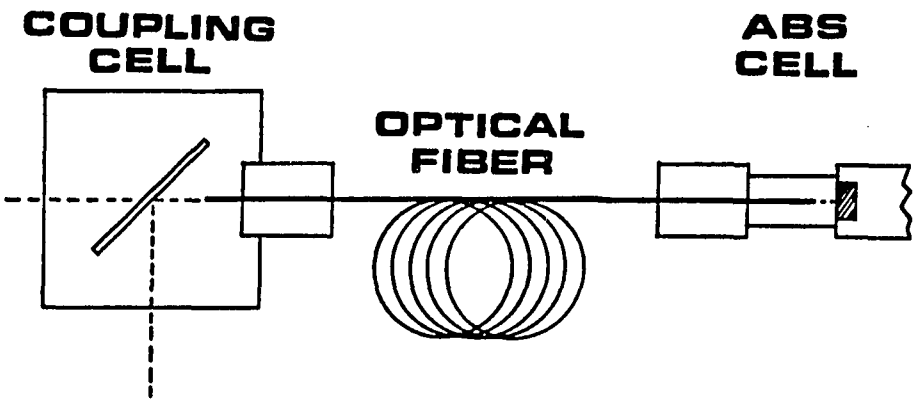

Figure 4. Interfaces in single-fiber optic absorbance probe
The light path is represented by a dotted line.

optical fiber, the percentage of reflected light is significantly reduced. For an optical fiber (n = 1.48) in cyclohexane (n = 1.43) the amount of stray light, ρ = 0.03%. Techniques to match refractive index are well known and form the basis for anti-reflection coated optical components.

Refractive index matching at the coupling end of the fiber can be easily implemented to reduce stray light. The stray light at the absorbance cell interface cannot be reduced so conveniently. For applications where the fiber is to be inserted into aqueous solutions the amount of stray light is about 10% larger than in cyclohexane due to the lower refractive index of water. The absorbance cell environment cannot be easily adjusted by refractive index matching to reduce reflected light without changing the nature of the sample. Therefore, the primary contribution to stray light in single fiber optic probes is from reflections at the fiber-absorbance cell interface. For single fiber applications this is an inherent problem that contributes to stray light. Other means to reduce stray light which are different from refractive index matching are required.

We demonstrate the use of phase modulation to time-resolve the analytical signal from the background. In this arrangement a long length of fiber is used as a delay line so that light that must pass through the optical fiber reaches the detector at a later time than light which is propagating outside the fiber.

The operating principle of an optical delay line is based on the difference of the velocity of light, ν, in a fiber and in air, as

given by

$$v = c/n \tag{5}$$

In equation 5, c and n take their usual convention of speed of light in a vacuum and refractive index, respectively. For light propagating in air (n = 1.00) the velocity of light is equal to 3 x 10^8 m/sec. When light must pass through an optical fiber (n = 1.48) its velocity is reduced to 2 x 10^8 m/sec.

We can calculate the delay in arrival time, t, of a pulse of light which must pass through length of fiber, ℓ:

$$f = v/4\ell \tag{6}$$

For a 200-m length of fiber the pulse is delayed 1 usec.

Optical delay lines based on fibers have been used for radio frequency and microwave signal processing (59,60) and to study transient photochemical phenomena (61). Analytical chemical applications of delay lines include background reduction in time-resolved fluorescence (62,63) and time-of-flight optical spectrometry (64). In the former, an optical fiber does not delay the signal, but rather, the light is forced to travel a longer path, which briefly delays the arrival at the detector. In the latter, differences in wavelength propagation of light through an optical fiber are exploited, so that the fiber acts as the dispersive element in a spectrometer, rather than a prism or diffraction grating.

The primary advantage to using an optical delay line in a fiber

absorbance probe is that the background can be removed from the analytical signal. If the light entering the fiber probe is modulated, light reflected at the fiber interface will be in phase with the modulation frequency. If an optical delay line is used, light passing through the sample is delayed in time according to equation 6.

In this experiment we match the length of fiber to the modulation frequency so that the light that passes through the sample reaches the detector at 90° out of phase with the backscattered radiation. Then a lock-in amplifier (LIA) can be used to distinguish the two signals. The modulation frequency, f, can be related to the length of fiber, ℓ, required to produce a 90° phase shift by the following equation:

$$f = \nu/4\ell \qquad (7)$$

From equation 7 we can calculate that for 100 meters of optical fiber (n = 1.48) the signal must be modulated at 500 kHz to produce a quarter-cycle phase shift.

The function of lock-in detection in subtracting the background signal is illustrated in Figure 5. In simple terms, the function of a LIA is to calculate the difference between separate phase regions within one cycle of a signal. If the LIA is used to differentiate two half-cycles from each other, as in Figure 5, a 90° phase shifted signal is present with equal components contributing to each phase region being compared. A phase shift of more or less than 90° does not give complete background cancellation.

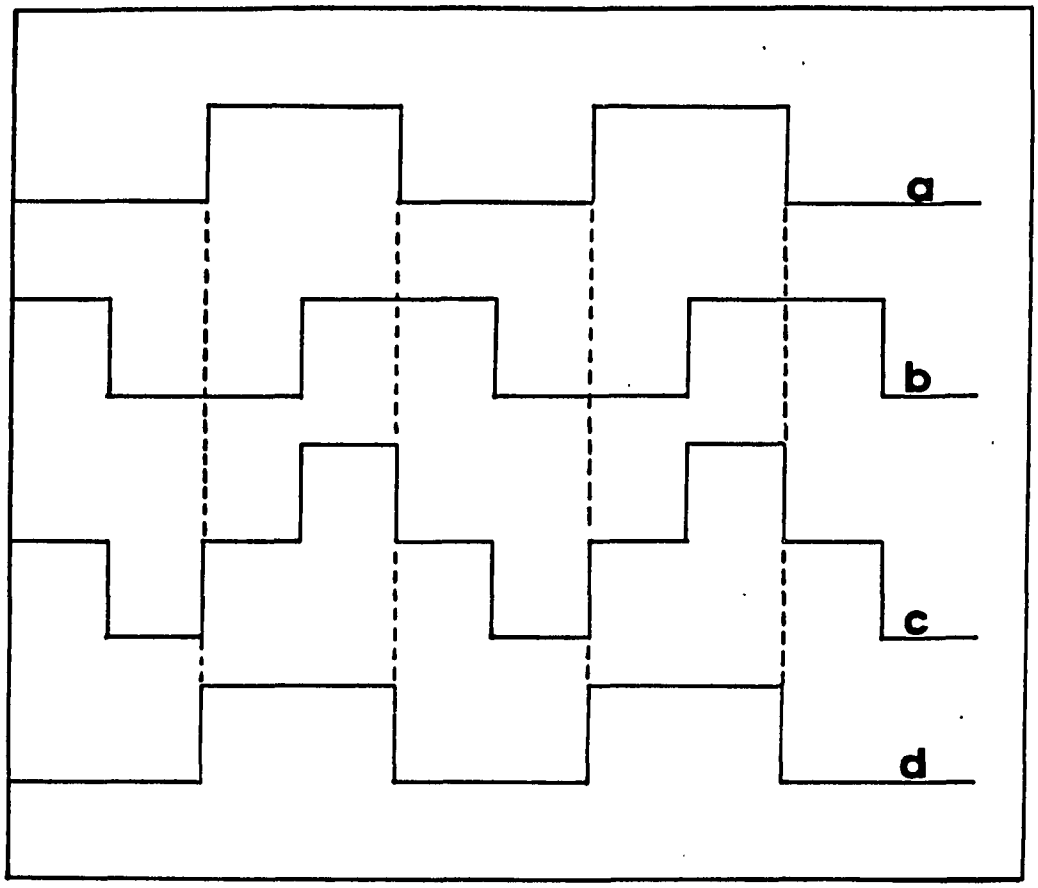

Figure 5. Contributing signals processed at the LIA
These signals are: a) signal from the absorbance cell, b) background signal due to stray light, 90° out of phase due to optical delay, c) sum of signals a and b, d) LIA signal as difference between the two half-cycles of c.

Experimental

The experimental arrangement to detect absorbance is shown in Figure 6. A He-Ne laser (Melles Griot, San Marcos, CA, model 05-LPL-540) is modulated into two beams with a Bragg cell (Coherent Associates, Danbury, CT, models 304 and 305D). The Bragg cell is driven by a signal generator (Wavetek, San Diego, CA, model 162) at 850 kHz. An aperture of 0.099 inches in diameter, made in-house, was positioned to pass the first-order beam from the Bragg cell, blocking all other orders. A 1/2" diameter 3-cm focal length lens (Oriel, Stratford, CT) was used to focus the first-order beam into the coupling cell containing one end of a 30-meter length of optical fiber. This length of fiber was wound around a spool and the other end was mounted into the absorbance cell. The reflected light was collected with a 1" diameter 5-cm f.l. lens (Oriel, Stratford, CT) and directed to a PMT (Hamamatsu, Middlesex, NJ, model R928), operated at 500 V by a high-voltage power supply (Cosmic Radiation Labs, Bellport, NY, model 1001B Spectrastat). The output of the PMT is sent to a high-frequency lock-in amplifier with 50 Ω input termination (EG&G, Princeton Applied Research, Princeton, NJ, model 520Z), and to a voltmeter (Keithley, Cleveland, OH, model 155). The outputs of the lock-in (with 1 sec time constant) and the voltmeter were sent to a computer (Digital Equipment, Maynard MA, model PDP 11/10 with LPS-11 laboratory interface). All optical components are mounted on a 2" thick optical table (Newport Research Corp., Fountain Valley, CA,

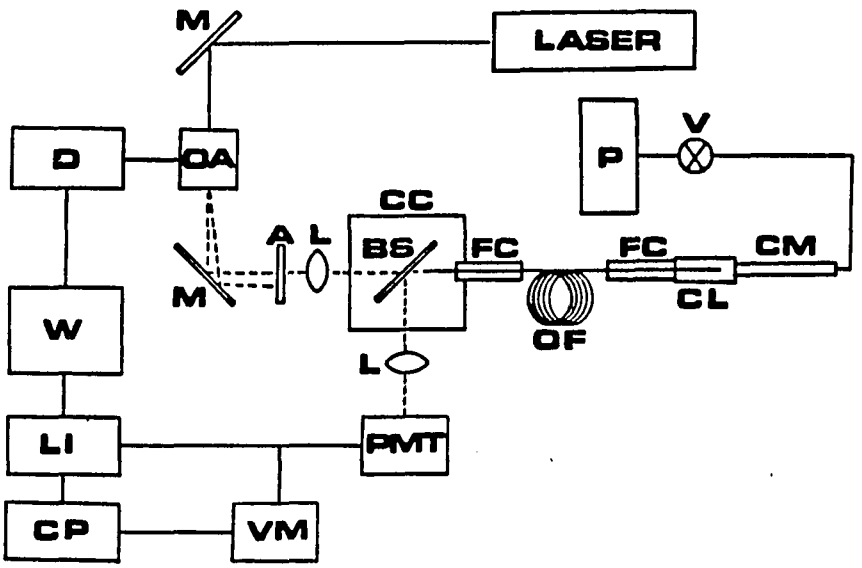

Figure 6. Fiber optic absorbance probe and chromatographic system P, pump; V, injection valve; CM microbore column; CL, absorbance cell; FC, fiber chuck; OF, optical fiber; CC, coupling cell; BS, beamsplitter; L, lens; A, aperture; M, mirror; OA, Bragg cell, Laser, HeNe laser; D, driver; W, square-wave generator, LI, lock-in amplifier; CP, computer; VM voltmeter; PMT, photomultiplier tube.

model LS-48).

Optical fiber

The 30 meters of optical fiber (Newport Research Corp., Fountain Valley, CA, model F-MLD) had a 100 u core and 140 u core and cladding diameter. The refractive index of the core was 1.4815. Approximately 5" of the protective coating on each end of the fiber was mechanically removed with a jacket stripper (Newport Research Corp, Fountain Valley, CA, model F-STP), leaving a fiber of 140 u diameter. The ends of the fiber were cleaved with a scribe (Newport Research Corp., Fountain Valley, CA, model F-CL-1). To ensure that a clean, flat surface had been produced, each end of the fiber was examined under a microscope.

Coupling cell

The cell, made in-house, consisted of a brass housing with two windows machined 90° from each other. A 1" diameter Inconel Beamsplitter (Oriel, Statford, CT) was mounted at 45° in the center of the cell. The cell windows were sealed by attaching microscope coverslips to the brass with epoxy. The optical fiber was mounted in the coupling cell with a 1/4" O.D. fiber chuck (Newport Research Corp., Fountain Valley, CA, model FPH-J). The chuck is inserted through a 1/4" opening, and a liquid-tight seal is made with an internal O-ring. The cell was filled with cyclohexane (Fisher, Fairlawn, NJ).

Absorbance cell

The other end of the fiber was inserted into a second fiber chuck, with a 1/4" swagelok nut attached to the end. The chuck was coupled to 1/16" O.D. chromatography tubing with a 1/4" to 1/16" reducing union. The tubing, 0.007" i.d. S.S. (Alltech, Deerfield, IL), forms the absorbance cell, the volume of which is determined by how far the fiber is positioned from the frit. For a 1.5 mm distance between frit and fiber, the cell volume is 0.037 ul with a pathlength of 3.0 mm. Standard replacement 2 u pore size frits (Alltech, Deerfield, IL) included with the column were polished to yield greater reflectivity. The frit is first mounted flat in an acrylic resin, and polished with 600 grit paper. Next it is polished with a vibratory polisher using a 0.3 u aluminum oxide abrasive. Finally, the mount is dissolved with acetone and the frit is washed in an ultrasonic bath of acetone.

The original frits were not replaced with polished frits for the chromatography columns used in this study. The chromatographic separation developed did not warrant a smaller cell. Therefore, the polished frit is seated in a 1/16" union with 3.5 cm of 0.007" i.d. tubing between it and the column frit. This extra length of tubing increases the total cell volume to 0.9 ul.

Chromatography

The chromatographic system used consists of a syringe pump (Isco, Lincoln NB, model uLC-500) and a 1.0 ul sample loop coupled to an

internal loop injection valve (Rheodyne, Berkeley, CA, Model 7410). For reverse-phase chromatography a 25 cm x 1 mm 5 u adsorbosphere C-18 chromatography column (Alltech Associates, Inc., Deerfield, IL) is used with an eluant system consisting of, by volume, 75% MeOH (Burdick and Jackson, Muskegon, MI, HPLC Grade) and 25% aqueous buffer of 4 mM citric acid (Fisher, Fairlawn, NJ). The water is deionized and purified by a commercial system (Millipore, Bedford, MA, Milli-O System). The pH of the eluant is adjusted to 7.4 with NaOH. Solutions of bromocresol Green (Hartman-Leddon Co., Philadelphia, PA) were prepared in the eluant. For normal phase chromatography a 25 cm x 1 mm 5 um microsphere silica column is used with cyclohexane as an eluant (Fisher, Fairlawn, NJ). Azulene (Aldrich Chemical Co., Milwaukee, WI) was dissolved in cyclohexane. All eluants were degassed under vacuum by ultrasonic agitation.

Results and Discussion

A convenient length of fiber for this work was 30 meters. The use of longer lengths was excluded, due to handling difficulties and increased attenuation. Shorter lengths of fiber could not be implemented due to pulse dispersion, which limits the maximum frequency of modulation. Since the configuration shown in Figure 6 was used, light had a double pass through the fiber, increasing the effective length to 60 meters. From equation 7 we calculate the theoretical modulation frequency required to achieve a 90° phase delay to be 844 kHz. Experimental verification of the modulation frequency

was accomplished by positioning the fiber in the absorbance cell at least 2 cm from the frit. At this distance light reflected at the frit and collected by the fiber was not detectable. In this position the major sources of light arriving at the PMT are from the modulated reflection at the cyclohexane-fiber interface within the coupling cell, and from the fiber-absorbance cell interface. This is the waveform that we used to set our zero on the LIA by maximizing the zero quadrant signal.

It is important to emphasize that this procedure is different than locking in on the modulated light being coupled into the probe. By moving the fiber away from the frit, while sustaining the same refractive index environment we are able to lock onto the true background signal. For the fiber in this position the magnitude of the signals in the 0^{o} and 90^{o} quadrants is indicative of the contribution of stray light. The lock-in signal was monitored in these quadrants for various frequencies when the fiber was positioned so that light was and was not being collected. The results of this study are summarized in Table 3.

When the fiber is not close enough to the frit to collect light, the analytical signal at 90^{o} is zero. This result indicates that not only have we removed the stray light contribution from the coupling cell, but also corrected for stray light within the absorbance cell. Therefore, when the fiber is positioned to collect light, the 90^{o} signal is due only to light which has interacted with the sample

Table 3.

LIA Quadrant Signals for Several Frequencies

Frequency kHz	Zero Quadrant (uV)	90° Quadrant pathlength (uV)	90° Quadrant 3 mm pathlength (uV)
700	+ 500	0	- 300
750	- 500	0	- 300
800	- 500	0	- 300
850	- 500	0	+ 300
900	- 500	0	+ 300

within the absorbance cell. Furthermore, we found that by locking onto the background signal the refractive index of the eluant in the absorbance cell did not affect the removal of the stray light contribution to the 90° signal. Therefore, using this method, one is not restricted in the refractive index within the probe cell. When applied to HPLC detection the probe would work equally well for normal and reverse phase eluant systems. Similarly, remote sensing applications benefit from dynamic stray light correction in any sample environment.

The data in Table 3 indicate that selection of the modulation frequency is quite flexible, since the 90° background contribution is zero for all frequencies encompassing the frequency expected to produce a quarter-cycle phase delay (844 kHz). This result is due to the complexity of the waveform. We did discover that the S/N ratio of the 90° signal with the fiber close to the frit depends on the modulation frequency used. The noise at equal pathlengths degrades by 30% in going from 850 kHz to higher or lower frequencies. This is probably related to better stray light correction when a quarter-cycle phase delay is produced. Based on the improved S/N and the observation that the magnitude of the 90° signal changes when the modulation frequency is close to the calculated frequency, we have chosen 850 kHz for this work.

In the complete arrangement shown in Figure 6, modulated at 850 kHz, we found that the S/N decreased for increasing pathlength. For a 3 mm pathlength we were able to achieve a baseline stability of 2 x

10^{-3}. This is consistent with a previous report of S/N in fiber optic based probes (54). The noise level was not flow sensitive between the flow rates of 10-100 ul/min.

The efficiency of coupling the laser light to the optical fiber was determined to be 95%. This factor takes into account an estimation of the attenuation of light by the fiber. The efficiency of coupling could be improved by using a shorter focal length lens, but this would require miniaturization of the coupling cell developed for this work. The polished frit was instrumental in providing enough light to establish a reasonable S/N for a 3 mm pathlength. Without the increased signal due to the polished frit, the best intensity S/N obtained for a 1 mm pathlength was 100. The increased reflectivity, demonstrated by photographs in Figure 7, enabled us to increase both the S/N and the pathlength.

We attempted to use a reference photodiode to adjust for laser intensity fluctuations, but found that the ratio of the lock-in and reference signals offered no improvement in baseline stability. The intensity stability of the HeNe laser alone was 0.1%. Even though this represents considerable flicker noise, the main contribution to noise in the fiber probe was apparently from mechanical instability of the optical fiber. It is likely that the S/N will improve if a design for rigidly mounting the fiber spool is developed. If this major source of noise is reduced, then flicker noise may become a factor.

For applications in capillary HPLC, even with limited baseline

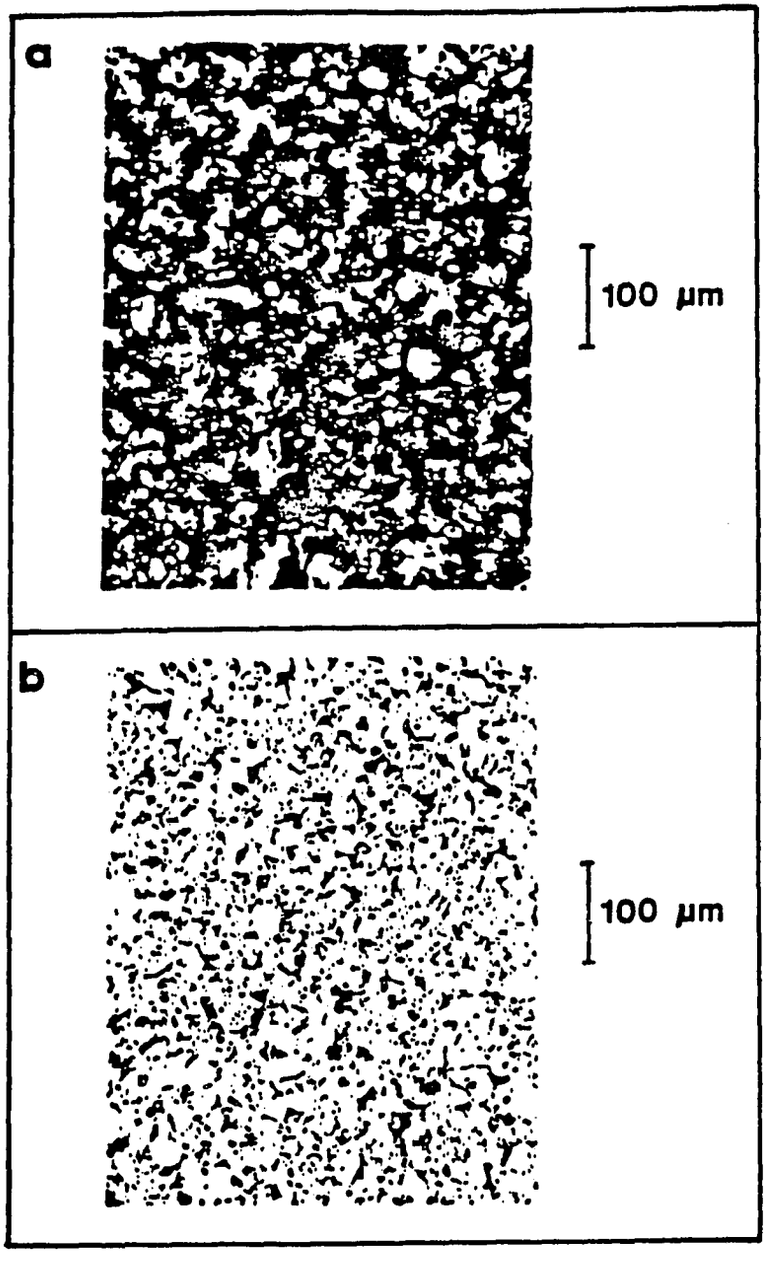

Figure 7. Magnified photographs of chromatography frits a) conventional frit, b) polished frit.

stability, the fiber probe represents an improvement in detectability due to increased pathlength. By calculating the ratio of absorbance, A, to pathlength, b, we can access the true detectability of the detector. To estimate the improvement we use as comparison a state-of-the-art capillary absorbance detector, for which the pathlength is perpendicular to eluant flow. The best detectability for a detector of this type has been demonstrated with capillary electrophoresis with an absorbance detectability of 1×10^{-4} a.u. for an 80-um pathlength (56). For this detector A/b is 1.3×10^{-2}. For our modulated fiber based absorbance detector with a 3 mm pathlength this ratio is 6.7×10^{-3} (S/N = 2). Therefore, even though the S/N is smaller for the fiber based detector, the detectability is actually better by a factor of two, due to the increased pathlength.

In order to assess the improvement made by the optical delay line in removing stray light, we compared absorbance chromatograms obtained with and without modulation. Bromocresol green was selected (BCG, MW = 698 g/mole) for reverse phase chromatographic studies because it was retained on a C_{18} column. Solutions of BCG in eluant were found to have a molar absorptivity of $\varepsilon = 38{,}000$ L/(mol cm) at 633 nm.

Figure 8 shows a chromatogram obtained as the output of the LIA. The first peak is due to the elution of BCG at a flow rate of 40 ul/min. The second peak is an injection disturbance which was observed only when eluant was injected. The mass detectability for BCG is 2 ng (S/N = 2). This correlates well with the detectability

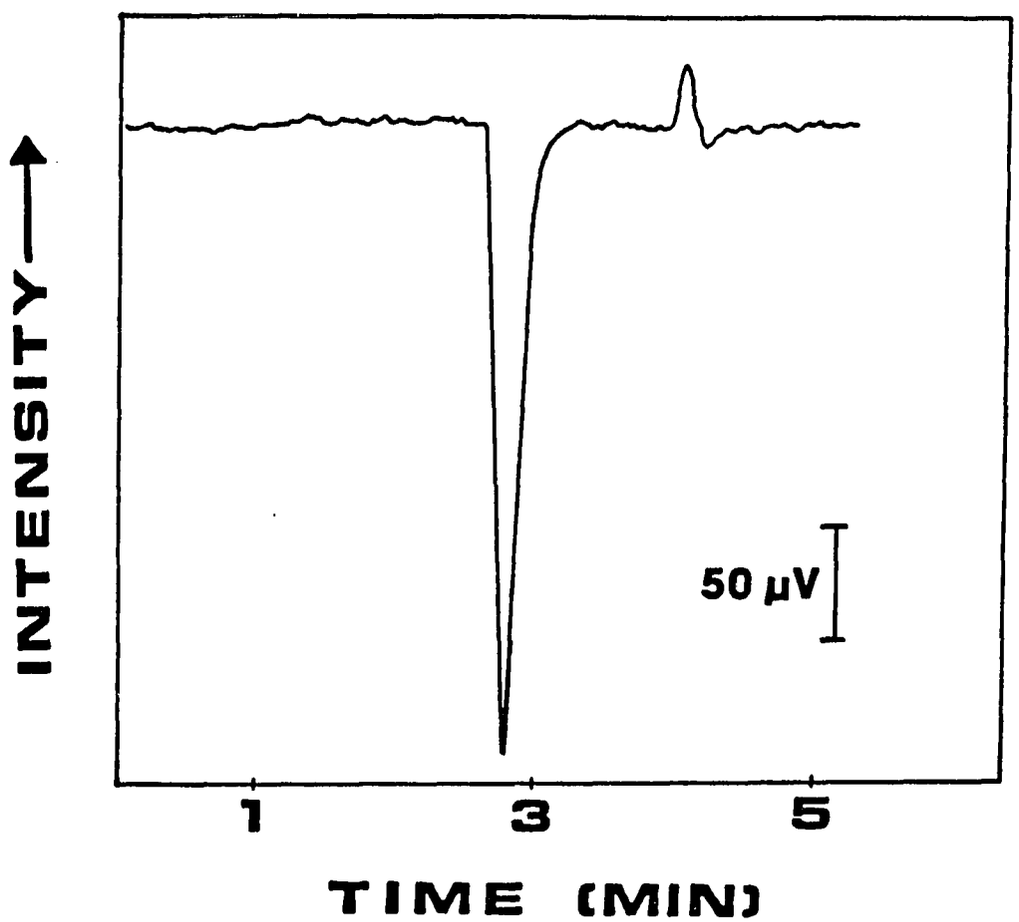

Figure 8. Modulated chromatogram for 3.9×10^{-4} M BCG
Injection loop, 1 ul; column 25 cm x 1 mm i.d. 5 um C_{18}; eluant, 40 ul/min 75:25 methanol:H_2O; I_o = 400 uV; I at peak = 110 uV.

calculated from the baseline stability. The output signal from the voltmeter, corresponding to the same injection as Figure 8, is shown in Figure 9.

The total integrated absorbance of the BCG chromatographic peak was calculated by summing the absorbance of each data point. The individual absorbance values were calculated from the relationship

$$A = \log I_o/I \qquad (8)$$

for each data point collected. The conventional definitions apply here, where I_o is the intensity of light detected with no absorbance and I is the intensity detected when the sample is absorbing light. The values of I and I_o used were the voltage values outputted from the LIA and voltmeter. These voltage values were adjusted for scale, rate of data acquisition and flow rate. For this calculation I_o was the average baseline value determined from 20 seconds of baseline data prior to the elution of the chromatographic peak.

Visual comparison of Figures 8 and 9 reveals a smaller absorbance peak resulting from the voltmeter signal. Verification that this difference is not due to the scale factor is accomplished by calculation of the total peak absorbance. A plot of total peak absorbance vs. BCG concentration for the LIA signal and voltmeter is provided in Figure 10. This plot indicates that not only are the total absorbance signals different but each plot has a different plots were obtained from the same injection and the same detector, with the only difference being how the PMT signal was processed.

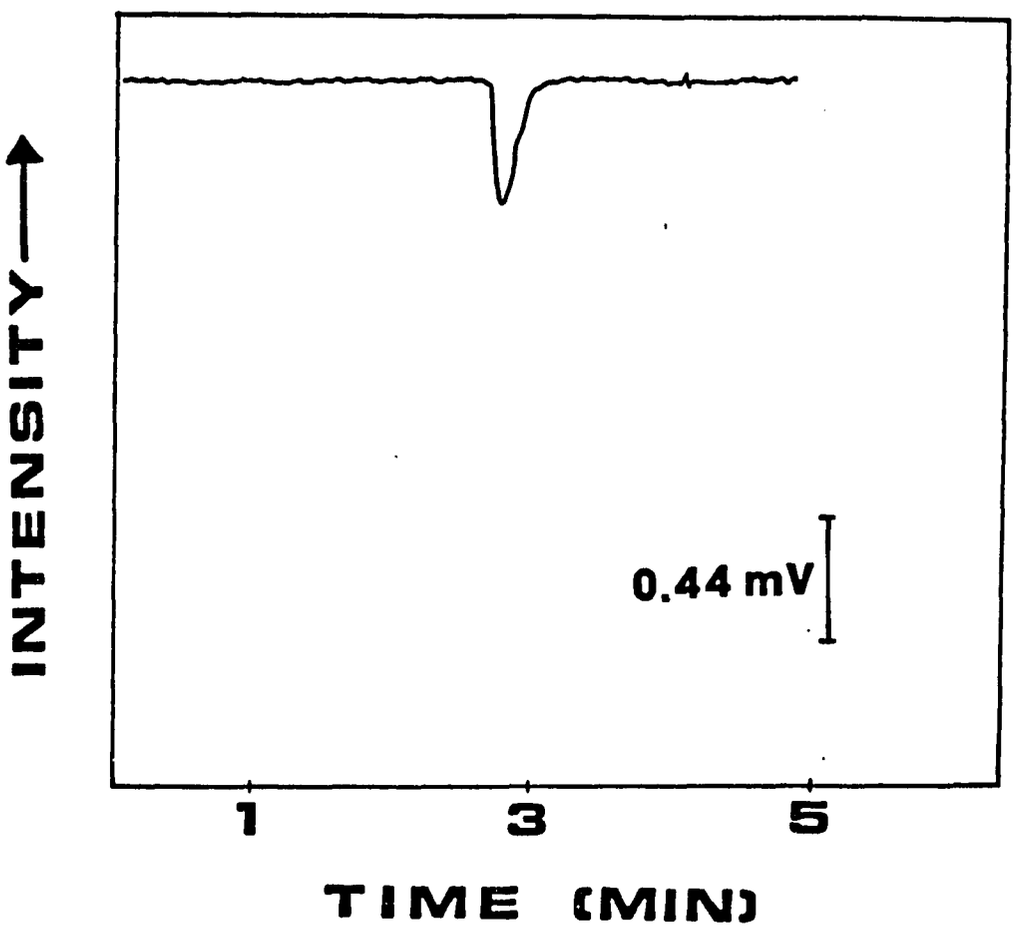

Figure 9. Non-modulated BCG chromatogram
For identical injection in Figure 8, except I_o = 1.2 mV; I at peak = 0.76 mV.

slope. It is important to emphasize that the data used to make these plots were obtained from the same injection and the same detector, with the only difference being how the PMT signal was processed.

The difference between curves a and b in Figure 10 is not an artifact of signal processing. First, the data were adjusted for scale factor differences. Second, we verified that splitting the output of the PMT simultaneously between the inputs of the LIA and the voltmeter had no effect on the signal of either device. Finally, we determined that the signal detection with the voltmeter in this mode is equivalent to the signal obtained with no modulation. To establish this we turned off the Bragg cell and used a neutral density filter to adjust the light intensity to the same level present with modulation. The voltmeter signal was analyzed identically to when the intensity was modulated. A plot of total absorbance vs. concentration was equivalent to Figure 10b. This result indicates that the signal from the voltmeter, even when the light intensity is modulated, may be regarded as non-modulated absorbance detection.

The difference between the curves in Figure 10 is due to stray light. Phase sensitive detection and an optical delay loop minimizes negative deviations from Beer's law. We see that when no modulation is used, stray light diminishes the absorbance signal. The magnitude of the decrease in signal due to stray light is related to the refractive index difference between the fiber and the absorbance cell environment. For aqueous chromatographic eluants this difference is

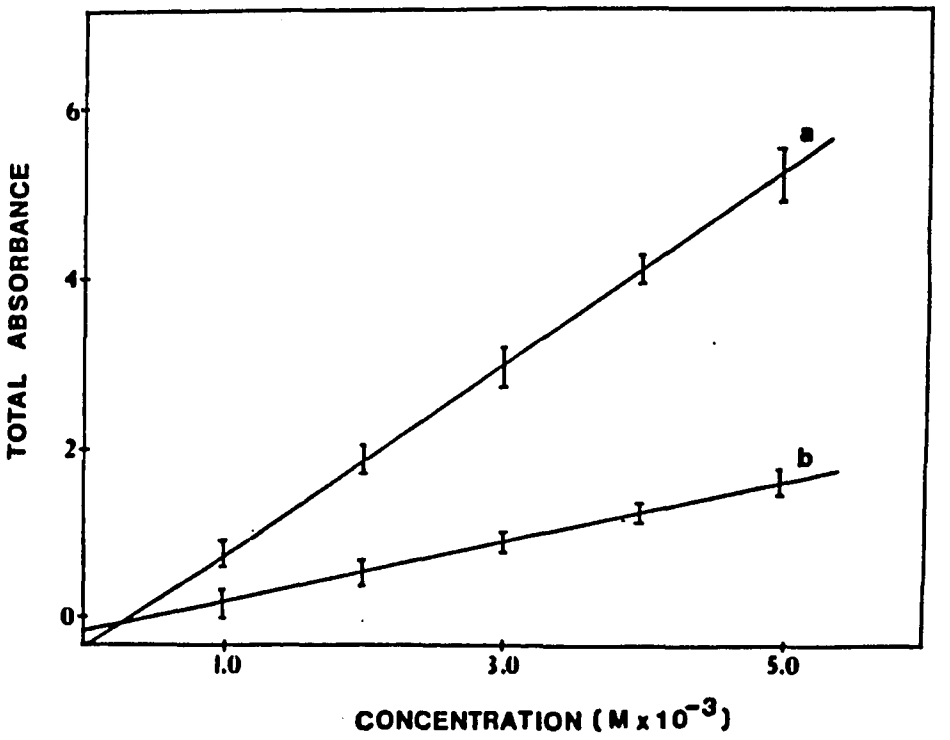

Figure 10. Beer's law plots of BCG absorbance signals
Plots represent 95% confidence intervals for three replicate measurements; a) modulated and b) non-modulated.

relatively large. When an eluant system with a smaller refractive index difference is used, we would expect a smaller deviation, due to less stray light.

In order to verify that stray light from the absorbance cell was primarily responsible for negative Beer's law behavior, we changed to a normal phase chromatographic system using cyclohexane as an eluant. Figure 11 shows the LIA signal following the elution of azulene (MW = 128, ε = 333 l/mol cm). The corresponding chromatogram from the voltmeter is provided in Figure 12. The plots of total absorbance vs. concentration for each device (Figure 13) verify that the deviation from Beer's law is smaller when cyclohexane is used as an eluant instead of an aqueous solution. This result elucidates that the main contribution to stray light in a fiber probe comes from the absorbance cell and confirms the utility of modulation with an optical delay loop in removing this portion of the absorbance signal.

The method we used to mount the optical fiber in the absorbance cell made it difficult to measure the pathlength accurately. We estimated it to be 3 mm for both normal and reverse phase chromatography. By using the slope of the Beer's law plot for the modulated data obtained by linear regression, together with the experimentally determined molar absorptivity, we can calculate the pathlength of the absorbance probe. For both normal and reverse phase chromatography b = 3.1 mm. These data, as well as the corresponding statics and regression equations, are summarized in Table 5. Since

Table 4.

Pathlength and Linear Regression Data for BCG and Azulene

Sample	Modulated slope, Beer's plot ± standard deviation	Non-modulated slope Beer's plot ± standard deviation	Calculated pathlength (cm), from modulated slope ± standard deviation
BCG	11663 ± 314	3629 ± 144	0.31 ± 0.01
Azulene	102 ± 3	77 ± 2	0.31 ± 0.03

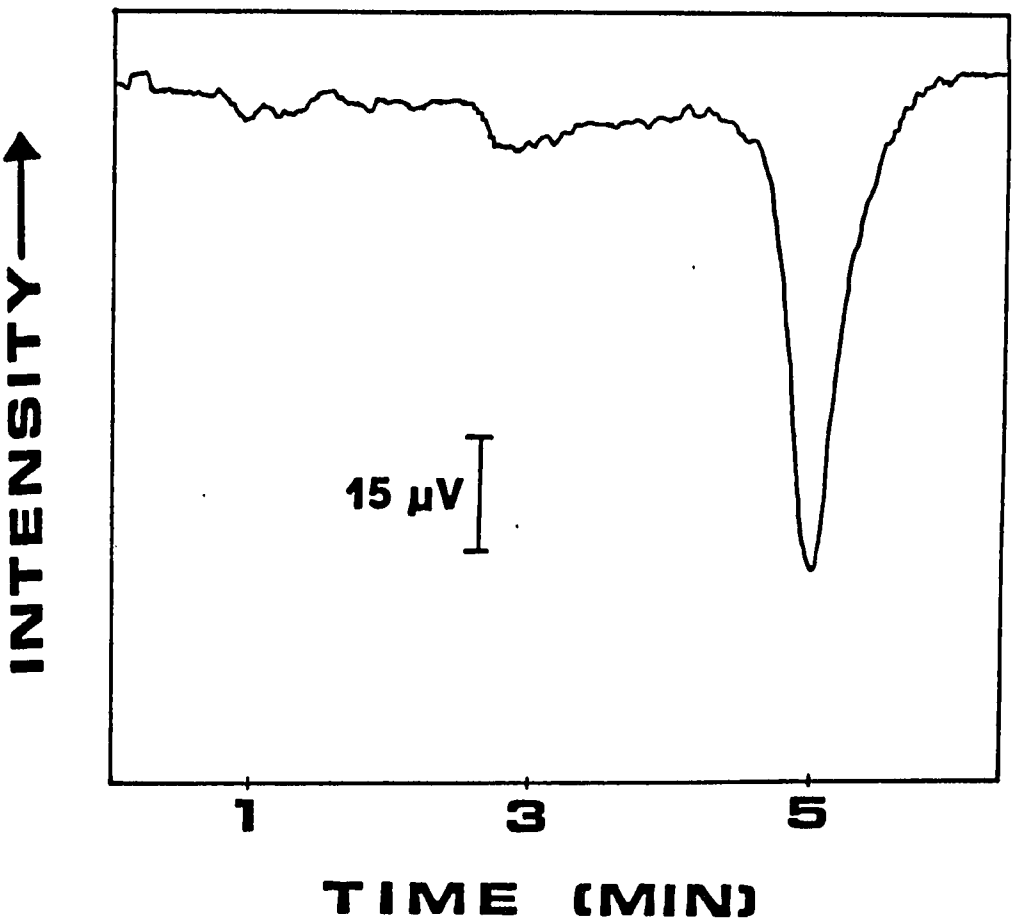

Figure 11. Modulated chromatogram for 1.58×10^{-2} M azulene Injection loop, 1 ul; column 25 cm x 1 mm i.d. 5 um silica; eluant, 45 ul/min cyclohexane; I_o = 400 uV; I at peak = 338 uV.

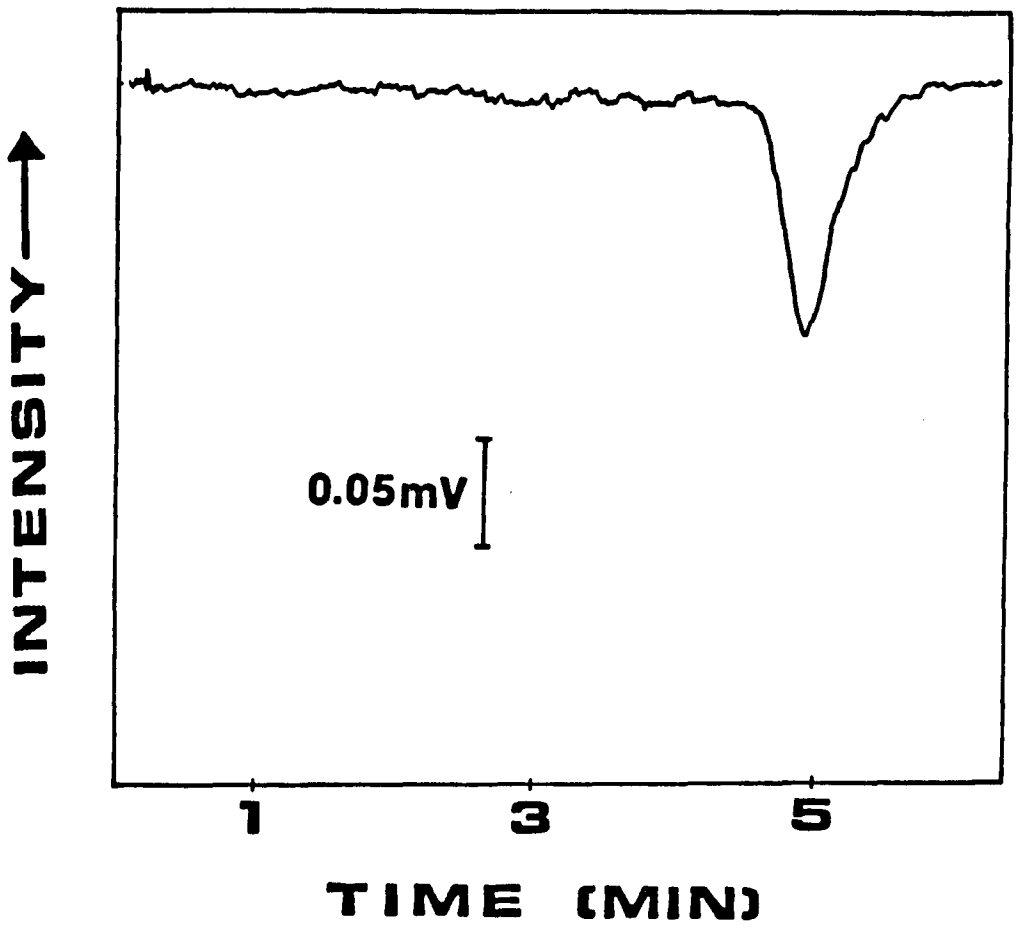

Figure 12. Non-modulated azulene chromatogram
For identical injection in Figure 11, except I_o = 0.87 mV;
I at peak = 0.86 mV.

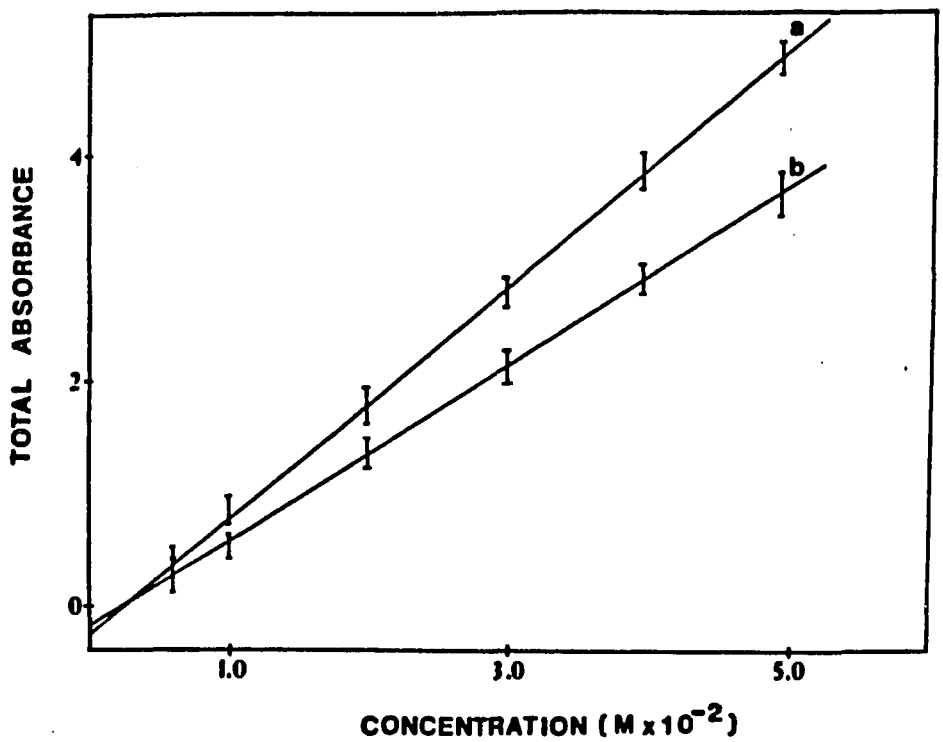

Figure 13. Beer's law plots of azulene absorbance signals
Plots represent 95% confidence intervals for three replicate measurements; a) modulated and b) non-modulated.

the pathlength was not known exactly, we cannot conclude unequivocally that the modulated probe is measuring the absolute absorbance of the sample without interference from stray light. However, since the pathlength calculated from the slope confirms the estimated value of the pathlength, it is reasonable to conclude that the absorbance calculated by the modulated optical delay method is very close to an absolute absorbance measurement. At the very least, this method demonstrates a marked improvement in stray light compensation for fiber probes.

If the original exit frit on the chromatographic column is used as the reflecting surface within the absorbance cell, the minimum cell volume for a 3 mm path is 0.049 ul. For capillary HPLC a detector volume this small is necessary to minimize peak broadening. For the microbore chromatographic systems utilized in this work a detector cell of this volume would offer no improvement in decreased peak broadening. Therefore, we did not replace the existing column frit with the highly reflective, specially polished version. Instead, we placed the polished frit in a chromatographic union coupled to the column exit. This arrangement increased the cell volume to 0.93 ul, which is highly suitable for microbore HPLC of the type described here.

In summary, we have demonstrated a unique improvement in fiber optic absorbance probes. The probe minimizes stray light and essentially provides absolute absorbance detection. The nature of the

sample environment will not alter stray light reduction. Therefore, the probe will be extremely useful in remote sensing and in-vivo applications. We have shown the usefulness of the probe in microbore HPLC, where a small cell volume and long pathlength are provided. The limiting factors here are fiber instability and perhaps laser flicker noise. Improvements in the probe should be possible if the fiber is mounted more rigidly and if the intensity instability of the light source is improved. The latter is possible if a sample and reference cell are used or a more stable light source, such as a semiconductor diode laser, is employed.

CHAPTER 3.

SINGLE LASER THERMAL LENS DETECTOR FOR MICROBORE LIQUID CHROMATOGRAPHY BASED ON HIGH-FREQUENCY MODULATION

Introduction

Since the invention of the laser, many applications to analytical measurements have been reported (65). Improvements over conventional light sources have been possible when one takes advantage of special properties of laser light. High power can lead to larger signals in laser-excited fluorescence (66) and thermo-optical effects (67), as well as new types of signals in, e.g., two-photon excited fluorescence (68). Coherence can enhance interferometric measurements (69). High resolution can provide unique information in atomic spectroscopy (70). Good collimation and polarization properties can improve polarimetric measurements (71). Short pulse durations allow temporal resolution of events (72).

Much less attention has been given to the disadvantages of using lasers for analytical measurements, i.e., those inherent properties that affect performance and not factors such as cost and convenience. The most important of these is the poor intensity stability of lasers. This is not surprising, since the output intensity depends exponentially on the gain of the laser medium, which in turn is excited by similar mechanisms as in conventional light sources. While one can often quite easily increase the measured signal in laser

experiments, noise also increases when lasers are used. Even though there may be a net gain in signal-to-noise ratio (S/N), a clear advantage may not be satisfactorily demonstrated. An example is fluorometry, where stray light and not signal strength is often the limiting factor to detection. Improvements are possible in laser-excited fluorometry only when optical designs are incorporated to reduce stray radiation (73-76).

One particular class of analytical measurement techniques has grown in application, due largely to the use of lasers. These methods, which are based on heat generated due to the absorption of radiation, are called photothermal measurements. Representative techniques which fall into this class include photoacoustic, photothermal deflection and thermal lens spectrometry. While all these techniques are based on radiationless decay processes following the absorption of light, the method by which the heat produced is measured varies. In photoacoustic spectrometry (PAS), heat produced due to thermal relaxation causes an acoustic signal which is directly related to the amount of light absorbed. In PAS a microphone indirectly measures the sample absorption (77). The photothermal and thermal lens methods differ from PAS in two ways. First, these techniques measure light, rather than sound, and second, unlike PAS, which can use a conventional light source, these require excitation sources which have a gaussian intensity profile such as a laser (78,79).

In both thermal lens and photothermal deflection spectrometry

(PTD), the uneven cross-sectional intensity distribution of laser beams gives rise to a larger amount of light absorbed in the center of the beam compared to the sides. The subsequent radiationless decay causes uneven heating of the sample cross-section through which the beam is passing. This heat creates a differential refractive index profile across the sample so that the sample acts as an optical element. The manner in which this optical element is probed differentiates the two techniques.

For thermal lens spectrometry the divergence of a laser beam as it passes through the optical element is monitored. In this case, the refractive index gradient acts as a diverging lens, causing a passing beam to expand or "bloom." An aperture placed between the sample and a photodetector passes a certain amount of light. When absorption occurs, a thermal lens develops, blooming of the beam occurs and less light reaches the detector. The generated thermal lens can be probed a number of ways. In one method the same laser beam which creates the thermal lens is monitored for blooming. This is a single laser, single beam arrangement. Alternatively, a two-laser system can be utilized in a pump/probe design. Here the pump laser creates the lens, which is then probed by a second laser. Measuring absorbance indirectly in either of these ways can provide an extremely sensitive method for probing small absorbances (80).

A PTD measurement is experimentally similar to that made using a pump/probe thermal lens arrangement (81,82). The geometry of the pump

and probe beams as they pass through the sample is the principal difference. The two beams traverse the sample crossed at a shallow angle and the probe beam is deflected, but not diverged, by the refractive index gradient caused by pump beam absorbance. The deflection is sampled by placing a knife-edge between the sample and detector. Photothermal deflection and thermal lens spectrometry actually differ because different regions of the refractive index gradient generated by the absorbance of laser light are sampled.

Of all the photothermal methods there is no clear leader in sensitivity. The advantages and disadvantages of each technique depend on the application. While PAS and PTD can be used for analysis of solid surfaces such as coal surfaces and thin layer chromatography plates (83,84), thermal lens spectrometry cannot be used for this application. For optical detection only the thermal lens method can use a single laser, an arrangement which can greatly simplify the instrumental design. Finally, the best published absorbance detection limit for thermal lens analysis of liquids is 8×10^{-8} a.u. This is slightly better than the 1×10^{-7} a.u. detectability reported for both PTD and PAS (85).

In recent years, thermal lens spectrometry (86) has become quite popular for measuring small absorptions in solutions, particularly in combination with liquid chromatography (LC). In principle, high laser powers can be used to increase the thermal lens effect for a given analyte concentration. However, since an intensity is being measured, some of the gain is negated by the intensity instability of the laser.

We note that the better commercial UV absorption detectors for LC can achieve limits of detection (LOD) of 1×10^{-4} au at S/N = 3 (87). Continuous lasers with sufficient powers for thermal lens spectrometry have inherent instabilities of 1%. This is about two orders of magnitude worse than well-regulated conventional light sources. Power stabilization circuits can reduce fluctuations to 0.1%. It is possible to use a reference photodiode to correct for intensity changes (88), but electronic normalization circuits can only produce compensation to the 0.1% level. The time dependence of a thermal lens (89) can be used to reduce certain types of noise, with some sacrifice in the time response due to the computation procedure. Alternatively, a second laser with better intensity stability (e.g., a HeNe laser) can be used to probe the thermal lens generated by a more powerful but less stable pump laser (90,91). The main difficulty is the alignment and the matching of the beams in the probe region, especially when small sample volumes are of interest. Even then, HeNe lasers are stable only to the 0.1% level at typical operating frequencies. The use of pulsed laser systems as a pump source in generating a thermal lens has also been investigated (92,93). Pulsed lasers provide improved detectability for analytes in the gas phase; however, an improvement is not recognized for liquid samples. It is fair to conclude that thermal lens spectrometry has not achieved its full potential for detecting small absorptions, due to the above problems.

The "ideal" thermal lens spectrometer, especially one suitable

for LC, seems to be one that has the following features. First, it should be based on a single laser (88,90,94-98) with sufficient output power to cause a definite increase in signal. A second laser only complicates the alignment without necessarily bringing real reductions in noise. Second, since intensity is measured, one must be able to achieve an intensity stability of 1×10^{-4} or better; i.e., the baseline must be stable to that extent. Otherwise the enhancement factor (86) in the thermal lens effect will not be fully utilized. Third, since the thermal lens takes time to develop to its full strength (99) and time to relax (86), the maximum signal is obtained when a continuous excitation (vs. chopped excitation) is employed. Furthermore, since a high chopping frequency degrades the thermal lens signal (97) and a very low chopping frequency is not compatible with LC, the steady-state thermal lens seems to be the best approach. Fourth, there should be only one beam passing through the sample cell. This avoids any critical alignment procedures or instabilities in alignment, especially in small-volume applications. Fifth, it is preferable, although not essential, to base detection on a lock-in amplifier, which conveniently provides a differential measurement with a narrow bandwidth.

Recently, we have shown that double-beam laser experiments can provide effective intensity stabilities in the 10^{-4} (100,101) to 10^{-6} (102) range if high-frequency modulation is used. In this report, we describe an optical arrangement for thermal lens spectrometry that satisfies all of the above-mentioned features, in part due to the

introduction of high-frequency modulation. Results as applied to microbore LC detection will be presented.

Experimental Section

The optical arrangement is shown in Figure 14. An argon ion laser (Control Laser, Orlando, FL, model 554A) operated between 50 mW and 500 mW at 514.5 nm is sent into an acousto-optical modulator (Coherent Associates, Danbury, CT, models 304 and 305D) driven by a square wave from a signal generator (Wavetek, San Diego, CA, model 162). About 60% of the beam is modulated into the first-order Bragg component at 150 kHz. A 15-cm f.l. lens (Oriel Corp., Stratford, CT, 41775) is placed immediately after the Bragg cell. This serves to focus the laser beam into the microcell and to further separate the deflected beams from the Bragg cell by forming a virtual image. The flow cell for the LC effluent, shown in Figure 15, is derived from an earlier design (103), except that a pie-shaped wedge is cut on one side to allow the passage of the positive orders of the deflections by the Bragg cell. The cell i.d. is 0.61 mm, giving a volume of 2.9 ul. The cell is positioned 17.5 cm from the lens, where the beam size and beam separation are optimized. A home-made aperture 1.1 mm in diameter (placed near the edge of a square plate to avoid blocking the reference beam) is located 31 cm from the lens to analyze the thermal lens signal. To provide rigidity and ease of alignment, the aperture is mounted on x-y translational stages (Aerotech, Pittsburgh, PA, ATS

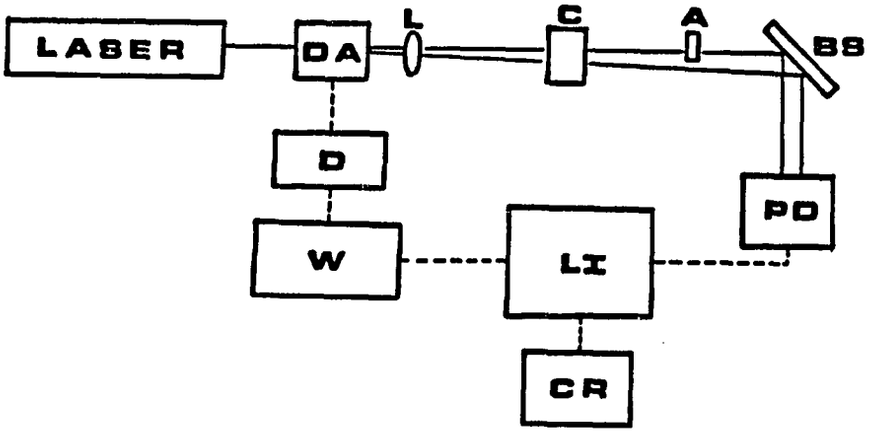

Figure 14. Experimental arrangement for high-frequency modulation in thermal lens measurements
LASER, Ar ion laser; OA, Bragg cell; L, lens; C, chromatographic flow cell; A, aperture; BS, beam splitter; PD photodiode; W, square-wave generator; LI, lock-in amplifier.

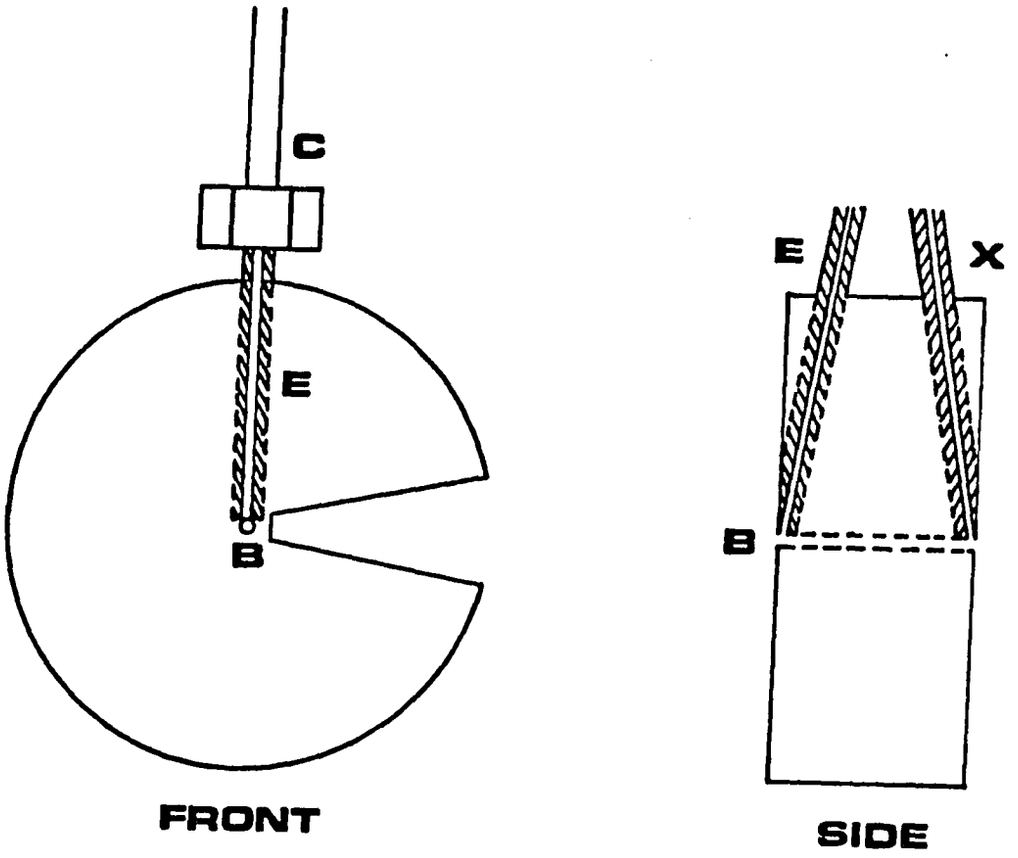

Figure 15. Flow cell for LC
Diameter, 2.54 cm; pathlength, 1 cm; B, bore 0.061 cm; E, entrance port (o.d. 0.16 cm, i.d. 0.013 cm); X, exit port (o.d. 0.16 cm, i.d. 0.013 cm); C, column. Distance between cell bore and pie-shaped clearance is 0.31 mm.

301). To reduce the intensity of light on the photodiode (Hamamatsu Corp., Middlesex, NJ, model S1790), a glass optical flat 10 mm thick and 38 mm in diameter (Oriel Corp., Stratford, CT, 44970) is used at 45° to send about 8% of the laser light to the photodiode. The active area of the photodiode is large enough (1 cm^2) to receive both the zeroth-order beam and the first-order beam. Output from the photodiode is sent directly (50 Ω termination) to a high-frequency lock-in amplifier (Princeton Applied Research, Princeton, NJ, model 5202) used at a 1-s time constant, and displayed on a chart recorder (Houston Instruments, Austin, TX, model 5000). All optical components are mounted on a 2" thick optical table (Newport Research Corp., Fountain Valley, CA, model LS-48).

The chromatographic system used consists of a syringe pump (ISCO, Lincoln, NB, model uLC-500), a 1.0 ul sample loop coupled to an internal loop injection valve (Rheodyne, Berkeley, CA, model 7410) and a 25 cm x 1 mm 5-um microsphere C_{18} chromatography column (Alltech Associates, Inc., Deerfield, IL). The eluent consists of 90% acetonitrile (Burdick and Jackson, Muskegon, MI, HPLC grade) and 10%, by volume, of an H_2O solution, initially deionized and purified with a commercial system (Millipore, Bedford, MA, Milli-Q System). All eluents were degassed under vacuum by using ultrasonic agitation. Other chemicals used are reagent grade without further purification. Absorptivity data for the stock solutions are measured in a conventional spectrophotometer (Shimadzu Corp., Kyoto, Japan, model UV-240). Computation was done on an Atari 1200 XL microcomputer in

BASIC.

Results and Discussion

Optimization of parameters

With the cell and the aperture removed in Figure 14, we are able to achieve a baseline stability of 1 x 10^{-5}. This represents the extent that flicker noise in the laser has been stabilized by the chosen modulation scheme. This is consistent with previous reports of the frequency distribution of noise in continuous lasers (102,104). The separation of the laser beam into two optical paths causes degradation in S/N compared to the single beam case (102), but except for circular dichroism (102) and polarimetry (103), two separate beams must be used to record the signal. Naturally, a Pockels cell plus a beam displacer can be used here instead of a Bragg cell (100). The higher modulation frequencies possible with a Pockels cell can further improve the flicker noise (102). However, flicker noise is not the limiting factor here--vide infra--and modulation at 150 kHz permits the use of more conventional lock-in amplifiers (e.g., Princeton Applied Research, Princeton, NJ, model HR-8).

With the cell in Figure 14 but with the aperture removed, the system functions as a conventional absorption spectrometer. The baseline stability was found to be 2 x 10^{-5} with or without eluent, a result of some degradation due to slight imbalance between the two beams. Liquid flow in the cell in the tens of ul per min. did not

affect the S/N ratio. At this cell i.d. and position relative to the beam waist, the laser beam clears the cell walls without any difficulties. When the cell is moved further away from the beam waist, alignment for this cell i.d. becomes difficult without introducing additional aperture effects (and additional noise) into the beam. So the position of the cell was not optimized with reference to the thermal lens effect, which dictates a maximum signal when the cell is 3 confocal parameters away from the beam waist (105,106). We estimate that the present signal is about 80% of that at the maximum, which is a good compromise to achieve the best intensity stability and ease of alignment. For smaller cell volumes or to allow placement at one confocal parameter from the beam waist, a shorter focal-length lens must be used. Using the Pockels cell in a similar modulation scheme (102), we have achieved on occasion an intensity stability through the flow cell of 5×10^{-6} at higher modulation frequencies. This shows that high-frequency modulation can be used with laser sources to provide intensity measurements at N/S of 5×10^{-6}, which is equivalent to an absorbance LOD of 7×10^{-6}, (S/N = 3).

The aperture size here is relatively large compared to those in other studies. To justify this choice, we have examined in more detail the dependence of the measured signal on the aperture size. We start by assuming a gaussian intensity distribution for the beam, which is characteristic of the TEM_{oo} mode output from our laser. So,

$$I(r) = I_o\, e^{-2(r/\omega)^2} \tag{9}$$

where I_o is the intensity of the laser at the center, r is the distance from the center, and ω is the characteristic beam waist. An aperture of radius R in the thermal lens experiment essentially passes all the light from r = o to r = R but blocks the rest. Equation 9 is a one-dimensional intensity distribution, and must be integrated in two dimensions to produce the transmitted intensity. One notes that at a distance r to r + Δr from the center, the area of the beam is given by $2\pi r$ due to the cylindrical symmetry of the beam. So

$$I(o + R) = I_o 2\pi \int_o^R re^{-2(r/\omega)^2}\, dr \tag{10}$$

Equation 10 can be evaluated in closed form, so that the fraction of light transmitted through the aperture, T, is given by

$$T = 1 - e^{-2\,(R^2/\omega^2)} \tag{11}$$

The relative sensitivity, S of the measurement is given by the change of transmitted intensity for a given (small) change in ω, $\Delta\omega$.

$$S = \left(\frac{\delta T}{\delta \omega}\right)\Delta\omega = -4\frac{R^2\Delta\omega}{\omega^3}\; e^{-2\;\frac{R^2}{\omega^2}} \tag{12}$$

If flicker noise (intensity instability in the laser) is the dominant

contributor to baseline fluctuations, the relative figure of merit, F, is given by

$$F = S/T \tag{13}$$

The results of the calculations based on equations (11) through (13) for various aperture sizes are shown in Table 6. We note that only the relative sizes of R and ω are important, so that a large aperture positioned further away from the beam waist produces identical results to a smaller aperture positioned closer to the beam waist. If the optical table is much more rigid than the aperture holder, then it is desirable to use larger apertures further away to minimize the effect of vibrations.

Table 5 shows that the maximum thermal lens signal is obtained when $R = 0.7\omega$. This is different from $R = \omega$ in the one-dimensional case. The maximum flicker-noise-limited S/N, however, is obtained with R as small as possible (large enough to make shot noise negligible); i.e., measuring the intensity change at beam center. When an aperture of size R = 0.75 (as judged from the transmitted intensity) is used in Figure 1 without the cell, the measured N/S of the intensity is about 5×10^{-4}. Using the aperture results in noise substantially larger than the flicker noise of 1×10^{-5}. This is because the aperture samples the pointing instabilities in the laser. When $R = 1.15\ \omega$ is used, the measured N/S of the intensity is about 1×10^{-4}. The measured N/S seems to be proportional to the intensity that is <u>blocked</u> by the aperture, (1 - T) in Table 6. A possible

Table 5.

Effects of the Aperture Size R
on the Thermal Lens Signal

R/W	T (%)	S (x10^{-4})[a]	F (x10^{-4})[a]
0.1	2.0	1.96	9.82
0.2	7.7	7.38	9.53
0.3	16.5	15.0	9.06
0.4	27.4	23.2	8.43
0.5	39.3	30.3	7.66
0.6	51.3	35.0	6.79
0.7	62.5	36.8	5.86
0.8	72.2	35.6	4.91
0.9	80.2	32.1	3.99
1.0	86.5	27.1	3.13
1.1	91.1	21.5	2.36
1.2	94.4	16.2	1.72
1.3	96.6	11.5	1.20
1.4	98.0	7.78	0.80
1.5	98.9	5.00	0.51

[a] $\Delta\omega = 5 \times 10^{-3}$.

explanation is that beam pointing instability of our Ar ion laser is the main source of noise, and not its intensity instability. This is further confirmed by the observation of drift in the baseline whenever the alignment of the laser drifts, at constant power levels dictated by the intensity servo control circuit in the laser. If less of the beam is blocked, the fractional intensity change is less when the beam position shifts at a constant ω. So, optimization of the aperture here should be with reference to S and not F in Table 6. In going from $R = 0.75\omega$ to $R = 1.15\ \omega$, we have reduced the sensitivity S by a factor of 2 but have reduced the alignment-induced noise by a factor of 5. Increasing R further to $1.35\ \Omega$, according to Table 6, reduces the sensitivity S by another factor of 2 and the noise (1 - T) by another factor of two. No further gain in real S/N is possible. So, the aperture size was chosen to be 1.15 multiplied by ω (as measured by T) for all subsequent experiments.

When an empty cell and the aperture in Figure 14 are in place, the baseline fluctuations are identical to those with the aperture alone, showing that the latter is the primary source of noise. When the eluent is then introduced into the cell at typical LC flow rates, the noise increases from 1×10^{-4} to 2×10^{-4}. However, this is because background absorption by the eluent causes the beam size ω at the aperture to increase; i.e., a background thermal lens effect. By moving the aperture away from the cell so that once again R = 1.15 multiplied by ω the stability of 1×10^{-4} was reestablished. Since

the background signal can be corrected for, no differential measurement (107) was needed.

In the complete arrangement as shown in Figure 14, we found that noise depends on the particular laser line used. The noise at equal powers degrades by a factor of 2 in going from 514.5 nm to 488 nm, with 476.5 nm intermediate between the two and 496.5 nm slightly worse still. The effect is not monotonic with decreasing wavelength, so that background absorption by the solvent cannot be used to explain this. Most probably the intensity stability and beam-pointing stability of the laser vary from one line to the next because of differences in threshold, gain, and operating current (tube temperature). Therefore 514.5 nm was chosen for all subsequent work, although this choice might be different, given another laser.

The particular optical arrangement in Figure 14 is designed to balance the effects of noise on the reference (+1) order) and the sample (zeroth order) beams as much as possible. A large displacement of the two beams is achieved if a beam-splitter is added to redirect one of them. However, vibrations in the beam-splitter will surely add noise. The one beam-splitter used is deliberately placed after the aperture, so it does not add alignment noise to the system. A large-area photodiode is chosen to allow collection of both beams, and avoids imbalance (if two separate detectors are used) and alignment fluctuations. The saturation point of this diode is about 5 mW, so a beam-splitter must be used to allow high laser powers in the sample cell. In practice, the Bragg cell modulates only 60-70% of the light,

so that a DC component exists in the zeroth order beam. This is no problem since the thermal lens needs high power in any case, and the steady state signal is insensitive to whether the excitation is truly continuous (DC component) or pseudo-continuous (modulated component). The sample and reference beams are not equal in intensity at the photodiode. This is because natural reflection at the cell windows and the presence of the aperture reduces the intensity of the sample beam. Some compensation is achieved, since the modulated light is distributed into the -1 (2%), +1 (96%) and +2 (2%) orders and only the +1 order is imaged onto the photodiode. An electronic offset is used at the lock-in amplifier rather than an attenuator on the +1 beam. Noise on this offset is not canceled in the lock-in amplifier. However, if the offset is small, one can still achieve stabilities of 1×10^{-4}. This explains why noise proportionately increases as the amount of light blocked, since that requires more electronic offset for detection.

Chromatographic studies

The compounds chosen are methyl red (MR, sodium salt, MW = 291) and benzopurpurin 4B (BPP, MW = 722). At the environment provided by the eluent, the former exists in both the neutral and ionic forms while the latter exists only in the ionic form. Solutions in the eluent at concentrations in the 10^{-5} M range are found to have molar absorptivities of $\varepsilon_M = 1.38 \times 10^4$ and $\varepsilon_B = 3.6 \times 10^4$ L/mol cm at 514.4 nm. In separate studies using analytical scale LC (4.6 mm i.d.

columns) and a commercial absorption detector (254 nm), it was determined that the two are cleanly separated with this eluent. While all of BPP elutes at short times, the MR components in the samples are eluted as two peaks, one at fairly short times and the other at very long times. These correspond to the ionic and the neutral forms of MR, respectively. No attempts were made to control the eluent pH to provide MR in only the ionic form, since a high pH is not compatible with the columns used.

Figure 16 shows a chromatogram obtained in our apparatus with the aperture removed. This is essentially a conventional absorption measurement. It is possible to predict the peak heights by noting that for small absorptions:

$$\Delta I = I_o \, 2.303 \, \varepsilon bc \qquad (14)$$

I_o is measured by blocking the reference beam to the photodiode, and is 23 mV for Figure 16. The peak heights for BPP and MR are 0.24 mV and 0.12 mV, respectively. The pathlength, b, is 1 cm. The two concentrations at the peaks are calculated by assuming a triangular peak shape to determine the half peak-volume, which gives a dilution factor for the injected sample (1 ul loop) of known concentration. Using equation 14, the peak signals are thus calculated to be 0.36 mV and 0.36 mV, respectively. The agreement for BPP between the predicted and the measured signals is acceptable, considering uncertainties in eluent flow rate, possible errors in sample

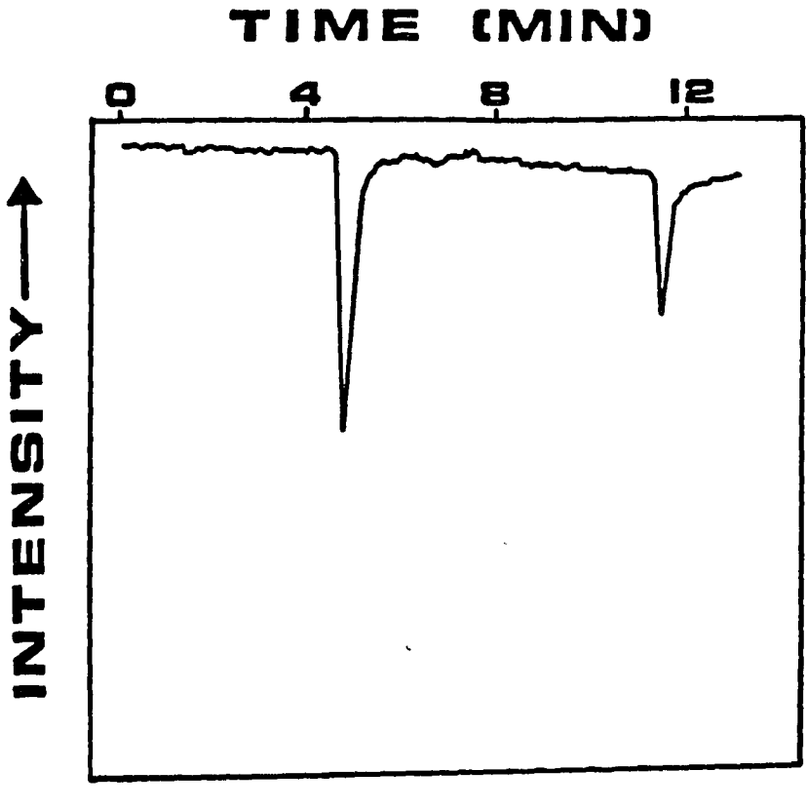

Figure 16. Absorption chromatogram for 1.9×10^{-6} M BPP and 4.9×10^{-6} MR
Injection loop, 1ul; column 25 cm x 1 mm i.d. 5-umC_{18}; eluent, 90:10 acetonitrile:H_2O; intensity, 69 mW; I_o = 23 mV; I (BPP) at peak = 0.24 mV.

preparation at these low concentrations, uncertainties in injection loop size and reproducibility, and approximations in measuring the peak area. For MR, the agreement is very poor. This is because MR is equilibrated between the two forms, and the peak in Figure 3 only reflects the ionic form. It is interesting that this discrepancy can be used to determine the extent of dissociation of MR, or other weak acids, in the environment provided by the eluent and the column. As discussed earlier, the absorbance detectability in this mode of operation is about 2×10^{-5} au (S/N = 3), which is slightly better than that using commercial absorption detectors. As expected, the absorption signal showed no power dependence at low (< 70 mW) powers. At high powers, the limited size of the photodiode acts as an unintentional aperture, distorting the chromatographic peak.

Figure 17 shows the chromatogram obtained when the aperture is also included in the optical path; i.e., the thermal-lens chromatogram. Note that even though the concentrations are smaller, the peaks are larger than those in Figure 16. The peak heights are 0.92 mV and 0.25 mV for BPP and MR, respectively. This clearly demonstrates the enhancement (86) in signal due to the thermal-lens effect. Two artifacts are noticeable in every chromatogram. At and immediately before injection, there is distinct disturbance to the baseline. This is due to manipulation of the injection valve, transmitting vibrations (misalignment) to the flow cell, which is directly connected to the end of the column. This disturbance disappears in a few seconds after injection, and does not affect the

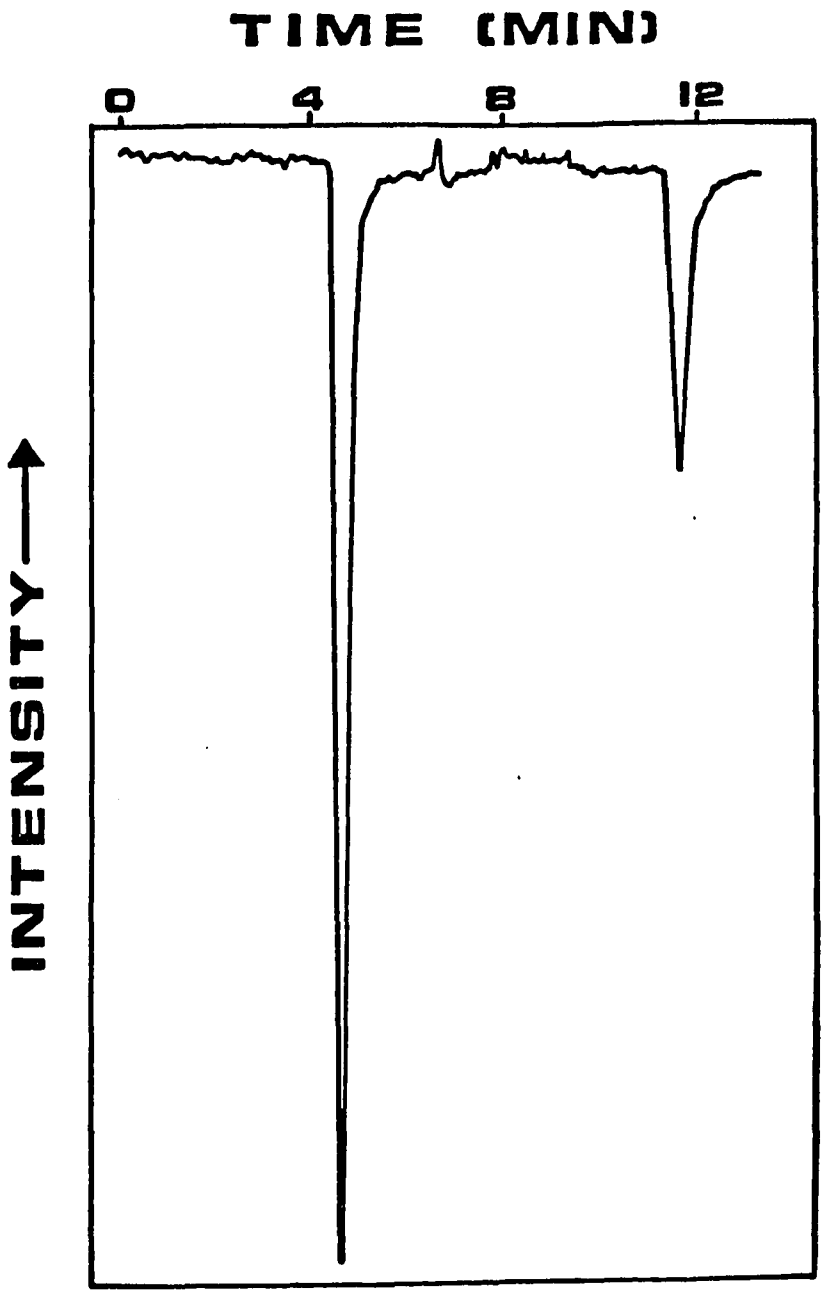

Figure 17. Thermal lens chromatogram for 7.5×10^{-7} M BPP and 1.95×10^{-6} M MR
Conditions identical to those in Figure 3, except that I (BPP) at peak = 0.92 mV.

main part of the chromatogram. At 6.5 min. into the chromatogram, a derivative-shaped disturbance to the baseline is present. This is not reproducible in size but reproducible in location. It occurs even if the eluent itself is injected into the system. These observations plus the fact that the event occurs after the void volume seem to indicate a pressure change at that point, a direct result of the brief interruption of flow of liquid when the injection valve is switched. A pressure change leads to a change in density and flow, thus affecting the beam alignment slightly.

The size of the peaks in Figure 17 naturally depends on laser power through the enhancement factor (86). In Table 6 we list the observed enhancement factors for the two compounds at various power levels (at the flow cell). It turns out that within this range of power, the relative intensity stability is always 1×10^{-4}, so that LOD improves at higher powers. It is possible to use even higher powers, but the Bragg cell used here loses diffraction efficiency (in effect a thermal lens at the acousto-optical crystal, smearing the acoustic standing wave). If this problem can be overcome, by, e.g., Pockels cell modulation, and if the light reaching the photodiode is proportionately reduced to avoid saturation, further gains should be possible. We note that Table 6 was derived by actually comparing a series of chromatograms of the type Figure 17 vs. Figure 16. So, uncertainties in injection loop size, changes in chromatographic behavior, concentrations of prepared solutions, equilibrium of eluted species, etc., are all compensated for. It is interesting to note

Table 6.

Thermal Lens Enhancement Factors for Peak Heights at Various Laser Powers

Power (mW)	MR	BPP
21	1.1	5.45
48	5.3	15.1
69	8.4	-[a]
90	18.2	24.0
108	22.7	-[a]
168	32.0	-[a]

[a]Substantial blooming observed, so normal absorption measurement is not possible.

that even at the limit of zero laser power, a signal will be observed here due to the normal loss of transmitted light in absorption experiments; i.e., Figure 16. This is not true of most published optical arrangements for thermal lens spectroscopy. The enhancement factors listed in Table 6 are corrected for this additional signal to compare with other published results (86). One must recognize that the actual enhancement in our experiments will be larger through this extra contribution. Essentially, 1.0 should be added to each number in Table 6. When these enhancement factors for BPP are plotted against laser power, a straight line is obtained with a slope of 0.26 per mW. This is to be compared to $E \simeq 1.0$ per mW for this mixture of water and acetonitrile (86). A factor of 2 in the discrepancy can be attributed to the fact that our aperture is operating at the half-sensitivity point (vide Table 6). The remaining deviation is due to cooling of the thermal lens because of eluent flow in the cell (replacement of the heated liquid), unoptimized location of the cell relative to the beam waist, and finite size of the cell diameter so that an infinite heat sink cannot be assumed. So, the agreement with expected enhancement for BPP is good. For MR, the slope for the data in Table 6 is 0.22 per mW, which is slightly less than that of BPP, but with large standard deviations and a large negative intercept. This is unexplained, since the operating conditions are identical to those for BPP. A plausible explanation is that MR is less efficient in converting the excitation energy into heat and therefore a lens in the solvent. There can also be a shift in ionic equilibrium on

electronic excitation, since at these laser powers and with such a large molar absorptivity, a large fraction of MR will be excited. Finally, the absorption may well be saturated at these power densities, decreasing the amount of energy deposited.

At the highest laser power used (90 mW at the cell) we have injected a solution containing 1.5×10^{-7} M BPP and 3.9×10^{-7} M MR. The S/N at the chromatographic peaks are 109 and 25, respectively. So LOD (injected amount) for BPP and MR are found to be 3.0 pg and 14 pg, respectively (S/N = 3). The latter has to be interpreted with caution because only the Na salt of MR is eluted in the peak shown, and the LOD refers to the total MR injected. In terms of absorbance detectability, the BPP peak shows LOD = 4×10^{-6} au (S/N = 3). These results compare favorably with other thermal lens reports in the literature despite the simplicity of the present design, when corrections for molar absorptivity, solvent, and chromatographic behavior are made. In order to verify that we were working within a linear range, we confirmed that over a range of 10 in concentration from this solution, the signal is linear. The full extent of the linear range was, however, not determined.

The cell used here is marginal for microbore LC, since the volume is about 1/6 of the peak volume of BPP. There is no problem in passing the beam at this location through a 1 ul flow cell (101), but much more critical alignment is required. As it is, the system is stable and the laser needs only to be warmed up and tuned from day to

day to achieve a stability of 1 x 10^{-4}. There is also a chance that the thermal lens causes clipping of the beam at the exit side of the cell, limiting the dynamic range. However, we did not observe clipping within the concentration range studied. Finally, a small i.d. will reduce the thermal lens signal because an infinite heat sink is not available. The solution to these problems is to use a still shorter focal length lens to reduce the beam waist to the point where the 1-cm optical pathlength is equal to the confocal distance. Judging from the MR peak in Figure 4, the plate number is 3800. This is a factor of 3 worse than the manufacturer's specifications, and is expected due to contributions from the cell volume and undesirable ionic interactions between these species and the column material. The latter contribution is particularly evident in the chromatograms as a slight tailing of the peaks. For a series of chromatograms at flow rates between 50 ul/min and 15 ul/min, we found that the signal for BPP degrades above 30 ul/min due to cooling as the liquid in the cell is replaced. So 20 ul/min is used in this work.

In summary, we have demonstrated the use of high frequency modulation in thermal lens spectrometry. The system is based on a single laser, is as stable in intensity as conventional light sources, is pseudo-continuous in excitation, is easy to align and to maintain in good alignment, and is based on lock-in detection. The LOD seems to be limited by the pointing stability of the laser relative to the aperture, a factor that will limit any thermal lens measurements in any case.

CHAPTER 4.

QUANTITATIVE GAS CHROMATOGRPHY WITHOUT ANALYTE IDENTIFICATION BY ULTRASONIC DETECTION

Introduction

The velocity of sound in a gas has for 70 years been a basis for gas analysis (108). The idea has been applied to gas chromatographic (GC) detection (109,110), leading to the commercial availability of an ultrasonic detector (111). The ultrasonic detector is a universal detector which measures changes in the speed of a sound wave traversing the effluent of a GC column by comparing the phase shift of the wave to a reference signal (112). Since other universal detectors, particularly the thermal conductivity detector, were already readily available and widely used, the ultrasonic detector has seen limited laboratory use. This is true even though the ultrasonic detector has a dynamic range of six orders of magnitude (113). For all GC detectors this range is equaled only by a mass spectrometer (114). Furthermore, the sensitivity of the ultrasonic detector, which is greater than other universal detectors, exceeds nanogram detection (114).

It is generally assumed that quantitative analysis must be preceded by identification of the unknown and subsequent preparation of a calibration curve from standards. We have recently shown that this approach is unnecessary (115). The new quantitative concept has been demonstrated in liquid chromatography (LC) using refractive index

(116), absorbance (117), conductivity (118), and indirect polarimetry (119) for detection. The extension of this idea to the gas phase is important, since roughly 50% of all current separations are performed using GC. In GC, even though retention times may change, the elution order of analytes does not change when different carrier gases are used, as can happen in LC upon changing the mobile phase. Therefore, correlation, or assignment of peaks, in a sample which contains two or more unidentified peaks as the carrier is changed is not a problem.

Quantitative GC without analyte identification has been reported using a mass detector (120), which is essentially a microbalance that monitors the gain in weight due to adsorption of the analyte onto activated charcoal. Detectability is poor, and is in the 1 ug range. The gas density detector for GC (121) has the potential of providing absolute quantitation (122). When quantitation is performed, a predictable response factor is obtained from the known molecular weights of the analyte and the carrier gas (123-125). In separate studies, such a detector has been adapted for determining molecular weights of analytes (126-128). Thus, by combining these two approaches, absolute quantitation is achieved. However, no experimental verification of this capability has been reported. Still, the gas density balance has poor detectability, slow response times, and occasionally nonlinear response (129), all of which limit its usefulness.

In this paper, we shall examine the properties and response

functions of an ultrasonic detector for GC. We shall show that good detectability is achievable, and that quantitation can be performed without analyte identification.

Theory

The response of an ultrasonic detector is well known (109). For a GC peak containing the carrier gas, c, and the analyte, x, the measure phase change, $\Delta\phi$, is predicted by:

$$\Delta\phi = 180 s f n_x \frac{M_c}{RT\gamma_c}^{1/2} \frac{M_x}{M_c} - 1 + \frac{Cp_x}{Cp_c}\frac{\gamma_c}{\gamma_x} - 1 \qquad (15)$$

where s is the distance between the transducers, f is the frequency of the sound wave, n is the mole fraction, M is the molecular weight, Cp is the molar heat capacity at constant pressure, and γ is the heat capacity ratio (constant pressure/constant volume). To arrive at equation 15, one assumes that both gases are ideal, the gas mixture is homogeneous, and the mole fraction n is small. These conditions are always satisfied in GC. If one integrates the response in equation 15 over the entire GC peak, one obtains a peak area, S_c, for the analyte in this carrier gas, such that

$$S_c K_c = N_x \frac{M_x}{M_c} - 1 + \frac{Cp_x}{Cp_c}\frac{\gamma_c}{\gamma_x} - 1 \qquad (16)$$

where N_x is the number of moles of analyte injected, and K_c is a proportionality constant which depends on the instrument and the carrier gas only (flow rate, temperature, molecular weight, and heat

capacity). One can simplify equation 16 by noting that for ideal gases, $C_p - C_v = R$. Still, equation 16 contains three unknowns, N_x, M_x and Cp_x. To determine the molar concentration, one must then obtain three chromatograms in three different carrier gases, and solve the three simultaneous equations of the form in equation 16. This way, the concentration is determined without standards and without analyte identification.

A further simplification can be introduced into equation 16 if the weight concentration, W_x, rather than the molar concentration, N_x, is used. We note that $W_x = N_x M_x$. So,

$$S_c K_c = W_x \frac{1}{M_c} + \frac{1}{M_x} \quad \frac{Cp_x - R}{Cp_c - R} - \frac{Cp_x}{Cp_c} - 1 \qquad (17)$$

By choosing two carrier gases with different molecular weights but identical molar heat capacities, e.g., two inert gases, one can obtain two independent equations for the two peak areas of the same analyte of the form

$$S_c K_c = W_x (F_c + F'_x) \qquad (18)$$

where F and F' are functions of the physical properties as specified in equation 17. Equation 18 has exactly the same form as equation 17 in reference (116), so that the procedure outlined there can be used to determine W_x without analyte identification.

If the molar concentration is to be determined, a third chromatogram must be obtained using a third carrier gas. It can be

seen from equations 17 and 18 that this third carrier gas must have a different value for Cp, or else the three simultaneous equations will not be independent. A reasonable choice of the third carrier gas is nitrogen, which has a predictable and well-behaved Cp value that is also different from that of the inert gases. An interesting result is that the quotient of the two concentrations, W_x/N_x, is the molecular weight of the analyte, and is useful qualitative information.

Experimental

All reagents used in this study were reagent grade. Solutions were prepared by pipetting well-defined volumes of the minor components into a volumetric flask, and filling to mark with the major component, methylisobutylketone.

A Tracor MT 150 Gas Chromatograph (Austin, TX) equipped with an ultrasonic detector and phase meter was used for the analysis, with 10 ft x 1/8 in stainless steel columns packed with 20% SP-2100/0.1% Carbowax 1500 on 100/120 Supelcoport (Supelco, Bellefonte, PA). The instrument, which was originally equipped with only a gas sampling valve, was modified to include a liquid injection port by using a stainless steel T-fitting. The injected sample volume was 5 ul throughout. Injection port, column, and detector temperatures were 125°C, 90°C, and 125°C, respectively. Research grade helium, nitrogen and krypton (Air Products, Allentown, PA) were used as carrier gases. Flow rates for He, Kr, and N_2 are 35, 40 and 26 ml/min, respectively. The back pressure of the detector was maintained at 20 psig.

The output of the detector was connected to a digital voltmeter (Keithley, Cleveland, OH, model 160B), the analog output of which was connected to a computer (Digital Equipment, Maynard, MA, model PDP11/10 with LPS-11 laboratory interface). The computer was programed to take readings every 0.05 sec and average a set of five before storing the information. A minimum of 80 of these averaged data values defines a peak. The area is determined by summation of the adjusted values above a chosen baseline for each peak. All areas were determined using averages of multiple (3 or more) injections. Linearity of the detector was confirmed for all analytes by analysis of successive dilutions of each solution.

Results and Discussion

Determination of W_x

As we have pointed out earlier (117), it is necessary to choose carrier gases and calibrating substances so that the simultaneous equations produce significant solutions. An inspection of equation 18 shows that one needs two monatomic gases that have as different reciprocal atomic weights as possible. This way, F'_x will be invariant, and F_c will be substantially different for the carrier gases. A good pair of carrier gases are helium and krypton. For these, $Cp_c = 5R/2$. The explicit form of the simultaneous equations is:

$$\text{He: } S_1K_1 = W_x \frac{1}{4} - \frac{1}{M_x}\frac{5}{3} - \frac{4Cp_x}{15R} \qquad (19)$$

$$\text{Kr: } S_2K_2 = W_x \frac{1}{84} - \frac{1}{M_x}\frac{5}{3} - \frac{4Cp_x}{15R} \qquad (20)$$

Subtracting equation 20 from equation 19,

$$W_x = (S_1K_1 - S_2K_2)/(\tfrac{1}{4} - \tfrac{1}{84}) \qquad (21)$$

The two constants can be evaluated if two independent calibrating substances of known weights are used to obtain peak areas in the same two carrier gases (117). The calibrating substances should have very different properties, F'_x, to make the determination of K_1 and K_2 reliable. The form of F'_x suggests that one of these should be a low molecular weight material with a large Cp, and the other should be a high molecular weight material with a small Cp. A convenient choice is then hexane and bromoform, respectively.

With these choices of carrier gases and calibrating substances, we can test the utility of equation 21 for predicting W_x without analyte identification. Four "unknown" compounds are chosen to span a range of molecular weights and heat capacities. They are acetonitrile, methylene bromide, carbon tetrachloride, and chlorobenzene. They form a convenient set because they are well separated on the GC column used in an isothermal run, together with the two chosen calibrating substances. Methylisobutylketone is used as the solvent for preparing the "unknown" mixtures because of the solubilities of these materials. Since the calibrating substances are in the same solution, errors due to variations in injection volume are

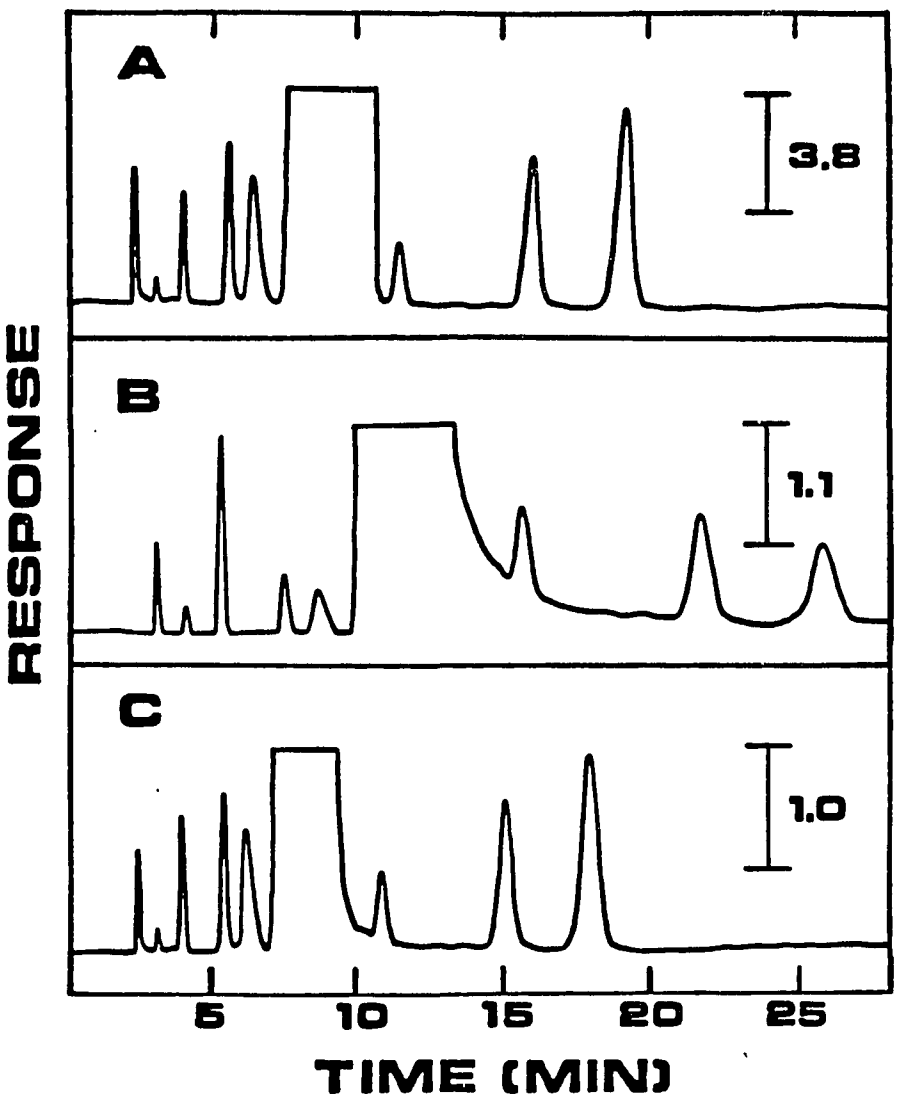

Figure 18. Ultrasonic chromatograms of sample mixture
Carrier gases for chromatograms a), b) and c) are He, Kr, and N_2, respectively. The features are, in the order of elution, CH_3CN, solvent impurity, C_6H_{14}, CCl_4, CH_2Br_2, solvent, solvent impurity, C_6H_5Cl, and $CHBr_3$.

eliminated. Still, from the reproducibility of multiple injections, we find that the injection volume is constant to 1%. The actual separation is shown in Figure 18 a-b. The retention times are different, due to the different flow rates used. The relative scale expansions are shown on the right. The responses are different, due to the nature of equations 19 and 20, and also due to the slightly different cell pressures used. Since all these are accounted for in the constants K_1 and K_2, they do not affect quantitation. In fact, K_1 and K_2 need only be determined once if the chromatographic conditions are kept constant for each carrier gas. The mechanisms for separation under these conditions are not expected to change with these carrier gases, so that the elution orders are maintained. Corresponding pairs of peaks from the two chromatograms can then be used as S_1 and S_2 when applying equation 21. The results of the W_x calculations are shown in Table 7, together with the known values in the sample.

To interpret the results in Table 7 property, one needs to estimate the uncertainties in the calculated values. This is done by following standard statistical procedures for propagation of errors, using the experimentally determined precision for each peak area measurement from three or more replicate experiments. These uncertainties are also shown in Table 7. Since the accuracy of K_1 and K_2 is critical, and since they need to be determined only once, the responses of the calibrating substances are obtained from five different samples spanning a ten-fold concentration range, with at least triplicate injections of each, and using several different scale

Table 7.

Quantitation of Analytes

	CH_3CN	CCl_4	CH_2Br_2	C_6H_5Cl
Expt. W_x(ug)	2.8 ± 0.2	6.5 ± 0.4	9.6 ± 0.6	13.3 ± 0.8
True W_x(ug)	2.9	6.0	9.4	12.4
Expt. N_x(nmoles)	73 ± 16	38 ± 39	76 ± 54	112 ± 96
True N_x(nmoles)	72	39	54	110

expansions on the instrument. The response for each was found to be linear with weight injected, with a correlation coefficient of 0.998 or better and a negligible zero intercept. The slopes of these lines are then used to calculate K_1 and K_2. Then, for each "unknown" compound in one particular mixture, the predictions of W_x are tabulated. We have also checked each of the "unknown" compounds for linearity of response over a ten-fold concentration range and obtained similar correlation coefficients. In other words, the predictions of W_x in all samples tested are equally good for each compound at each concentration.

Table 7 shows that the accuracy of the predictions is good and that the estimated uncertainty is about ± 6% in each case. Precision in W_x can be improved if more replicate injections are used, so that the peak areas and the injected volumes are more precise. Precision can also be improved if even better choices of carrier gases and calibrating materials are used. For example, ^3He should make a major difference in the contribution of F_c (replacing ^4He here), and an even heavier inert gas can be used (replacing Kr). In practice, these gases will be cost prohibitive. Hydrogen does have an even more favorable molecular weight, but its heat capacity is difficult to match in choosing the second carrier gas. As calibrating substances, larger alkanes can be used instead of hexane because of the higher heat capacity, and I_2 can be used instead of $CHBr_3$ because of the lower heat capacity. Still, the present choices clearly verify the applicability of this quantitation scheme.

Determination of N_x

As implied in equation 16, a third carrier gas must be used to obtain a third chromatogram for the unknown if Nx is to be determined. Nitrogen, being a diatomic, has a predictable heat capacity (=7R/2) that is different from the inert gases, and can be used. So,

$$N_2: \; S_3K_3 = N_x \frac{M_x}{28} - \frac{7}{5} + \frac{4Cp_x}{35_R} \qquad (22)$$

Since $W_x = N_xM_x$, equations 19, 20 and 22 can be used to solve for N_x. The same two calibrating substances, if eluted with N_2 as the carrier gas, will provide a value for K_3. Once K_3 is determined, the three unknowns N_x, M_x and Cp_x can be solved. The same test mixtures are therefore studied using N_2 as the carrier gas. The separation is shown in Figure 18c. From these chromatograms, the predicted N_x values for the "unknown" compounds are shown in Table 7, together with the known values. Again, the uncertainty estimates are derived from the propagation of errors based on the precisions in the peak area measurements.

A comparison of the predicted versus known N_x values shows that they agree within the estimated error limits. The error limits, however, are extremely large, except for the case of CH_3CN. This is to be expected, since N_2 does not have a heat capacity very different from the other gases, and the solutions to the simultaneous equations lose significance. For better precision in N_x determinations, a

better choice for the third carrier gas should be made; e.g., butane or SF_6. Using equation 16 and two calibrating substances, K_3 and Cp_3 can be determined for these carrier gases. Unfortunately, the particular ultrasonic detector used here will not function properly with these gases because of excessive damping of the sound wave. The acoustic cell length must be shortened to overcome this problem. Still, our data show that the concept is sound, and should be useful if the instrumentation is improved.

An interesting result is that the quotient, W_x/N_x, is the molecular weight of the analyte. The ultrasonic detector then becomes a "mass chromatograph." Naturally, this is not expected to replace mass spectrometers for GC detection, especially since the present uncertainties are large. On the other hand, the W_x values here show reasonable precision, and can be combined with a mass spectrometer to determine N_x to better precision, rather than relying on equation 22.

Detection limits

The response of the ultrasonic detector depends on the analyte as well as the carrier gas, according to equation 15. However, the determination of W_x here is of constant sensitivity as long as the molecular weight and the heat capacity of the analyte have been bracketed by the carrier gases. This is because of the fact that if the response is small in one carrier gas, it is necessarily large in the other carrier gas. We can then establish the detectability by considering only the response of hexane in He. The noise

(fluctuations in the baseline) is measured on a sensitive scale of the instrument with He alone flowing. The amount of hexane that produces a response three times that of this noise level is then the detectability. This is found to be 1 pg of hexane injected. The detectability rivals many of the more common GC detectors. It is not surprising that 1 pg is a substantially lower amount than that reported for the ultrasonic detector (114), since the earlier work only considered the detectability of H_2 in He, which is the worst possible case.

It should be emphasized that not all detectors can fit into the current quantitative scheme. Background signal, dynamic reserve, sensitivity and the mathematical equation relating signal to concentration are important factors in determining if the method is applicable to a specific detector. For example, the FID and the ECD cannot retain their sensitivity when a carrier gas with a high background is used. This is due to these detectors' small dynamic reserve. Gas phase RI detection could be used in this mode; however, its limited sensitivity restricts its application. Finally, although the thermal conductivity detector has good sensitivity and a large dynamic reserve, it cannot be used for this quantitative scheme. This is because there is not exact relationship relating the amount of sample present to the signal.

In summary, we have demonstrated the use of the ultrasonic detector for quantitation in GC without analyte identification, at a detectability comparable to some of the best GC detectors. This

unique information from the ultrasonic detector may increase its popularity as a routine analytical tool.

REFERENCES

1. Cassidy, H. C. "Fundamentals of Chromatography." Interscience Publishers, Inc.: New York, 1957, p. 3.

2. Runge, F. F. Ann. Phys. Chem., 1834, XVII, 65.

3. Tswett, M. Ber. Deut. Bot. Ges., 1906, XXIV, p. 316.

4. Martin, A. J. P.; Synge, R. L. M. Biochem. J., 1944, 38, 224-232.

5. Ettre, L. S.; Zlatkis, A. "75 Years of Chromatography, A Historical Dialog." Elsevier: Amsterdam, 1979.

6. Kirkland, J. J. Anal. Chem. 1971, 43, 36A.

7. Pryde, A. J. J. Chromatogr. Sci., 1974, 12, 486.

8. Knox, J. H. J. Chromatogr. Sci., 1980, 18, 453-461.

9. Tsuda, T.; Hibi, K.; Nakanishi, T.; Takeuchi, T.; Ishii, D. J. Chromatogr. , 1978, 158, 227-232.

10. Krejci, M.; Tesarik, K.; Pajurek, J. J. Chromatogr., 1980, 191, 17-23.

11. Locke, D. C. J. Chromatogr. Sci., 1973, 11, 120.

12. Jennings, W. "Gas Chromatography with Glass Capillary Columns." Academic Press: New York, 1980, p. 178.

13. Hibi, K.; Ishii, D.; Fujishima, I.; Takeuchi, T.; Nakanishi, T. J. High Res. Chromatogr. and Chromatogr. Comm. , 1978, 1, 21.

14. Menet, H. G.; Gareil, P. C.; Rosset, R. H. Anal. Chem., 1984, 56, 1770-1773.

15. Hare, P. E.; Gil-Av, E. Science, 1979, 204, 1226-1228.

16. Dom, H. C. Anal. Chem., 1984, 56, 747A-756A.

17. Bobbitt, D. R.; Yeung, E. S. Anal. Chem., 1985, 57, 271-274.

18. Windsor, D. L.; Denton, M. B.; J. Chromatogr. Sci., 1979, 17, 492.

19. Hartmann, C. H. Anal. Chem., 1971, 43, 113A-125A.

20. Krishnan, K.; Curbelo, R.; Chiha, P.; Noonan, R. C. J.

Chromatogr. Sci., 1973, 17, 413-416.

21. Small, H.; Miller, T. E. , Jr. Anal. Chem., 1982, 54, 462-469.

22. Yeung, E. S. J. Pharm. Biomed. Anal., 1984, 2, 255-263.

23. Synovec, R. E.; Yeung, E. S. Anal. Chem., 1983, 55, 1599-1603.

24. Wilson, S. A.; Yeung, E. S.; Bobbitt, D. R. Anal. Chem., 56, 1457-1460.

25. Cooper, S. D.; Moseley, M. A.; Peliggari, E. D. Anal. Chem., 57, 2469-2473.

26. Miller, D. A.; Skogerboe, K. J.; Grisrud, E. P. Anal. Chem. 1981, 53, 464-467.

27. Goldan, P. D.; Fehsenfeld, F. C.; Kuster, W. C.; Phillips, M. P.; Sievers, R. E. Anal. Chem., 1980, 1751-1754.

28. Dixson, J. B. Chimia, 1984, 38, 82-86.

29. Nota, G.; Palombari, R. J. Chromatogr., 1971, 62, 153.

30. Ohzeki, K.; Kambara, T.; Saitoh, K. J. Chromatogr., 1968, 38, 393.

31. McKinley, W. A. J. Anal. Toxicol. , 1981, 5, 209-215.

32. Mowery, R. A. J. Chromatogr. Sci., 1982, 20, 551-559.

33. Lunte, C. E.; Kissinger, P. T. Anal. Chem., 1984, 56, 658.

34. Polta, J. A.; Johnson, D. C. J. of Liq. Chromatogr., 1983, 6, 1727-1743.

35. Keuhl, D. T.; Griffiths, P. P. J. Chromatogr. Sci., 1979, 17, 471, 476.

36. Johnson, C. C.; Taylor, L. T. Anal. Chem., 1984, 56, 2642-2647.

37. Blakely, C. R.; Vestal, M. L. Anal. Chem., 1983, 55, 750.

38. Uden, P. C. NBS Spec. Publ., 1981, 618, 184-196.

39. Giering, L. P.; Horning, A. W. American Lab, November 1977, 113.

40. Vaughan, C. G.; Wheals, B. B.; Whitehouse, M. J. J. Chromatogr., 1973, 78, 203.

41. Pellizzari, E. D.; Sparachino, C. M. Anal. Chem., 1973, 45, 378.

42. Peterson, J. I.; Vurek, G. G.; Science, 1984, 224, 123-127.

43. Peterson, J. I.; Goldstein, S. R.; Fitzgerald, R. V.; Buckhold, D. K. Anal. Chem., 1980, 52, 864-869.

44. Johnson, C. C. Biomed. Sci.Instrum. , 1974, 10, 45.

45. Schultz, J. C.; Mansouri, S.; Goldstein, I. J. Diabetes Care, 1982, 5, 245.

46. Eckbreth, A. C. App. Opt., 1979, 18, 3215.

47. Chudyk, W. A.; Carrabba, M. M.; Kenny, J. E. Anal. Chem., 1985, 57, 1237, 1242.

48. Klainer, S.; Hirschfeld, T.; Bowman, H.; Milanovich, D.; Johnson, D. "Earth Sciences Division Annual Report," Lawrence Berkeley Laboratory, LBL 11981, November 1980.

49. Culshaw, B. "Optical Fibre Sensing and Signal Processing." Peter Peregrinus Ltd.: London, UK, 1984.

50. Seitz, W. R. Anal. Chem., 1984, 56, 16A-34A.

51. Zhuzun, Z.; Seitz, W. R. Anal. Chim. Acta, 1985, 171, 251-258.

52. Kirkbright, G. F.; Narayanaswamy, R.; Welti, N. A. Analyst, 109, 15-17.

53. Saari, L. A.; Seitz, W. R. Anal. Chem., 1982, 54, 821-823.

54. Coleman, J. T.; Eastham, J. F.; Sepaniak, M. J. Anal. Chem., 1984, 56, 2249-2251.

55. Sharpe, M. R. Anal. Chem., 1984, 56, 339a-356a.

56. Walbroehl, Y.; Jorgenson, J. W. J. Chromatogr., 1984, 315, 135-143.

57. Ishii, D.; Asai, K.; Hibi, K.; Jonokuchi, T.; Nagaya, M. J. Chromatogr., 1977, 144, 157-168.

58. Oleson, E. D. "Modern Optical Methods of Analysis." McGraw-Hill, Inc.: New York, 1975, p. 22.

59. Chang, C. T.; Cassaboom, J. A.; Taylor, H. F. Electronics Letters,

1977, 13, 670-680.

60. Wilner, K.; Van Den Heuvel, A. P. Proceedings of the IEEE, 1976, 64, 805-807.

61. Ewart, P. J. Phys. D: Appl. Phys. , 1981, 14, 9-11.

62. Russo, R. E.; Hieftje,G. M. Appl. Spec., 1982, 36, 92-99.

63. Russo, R. E.; Hieftje, G. M. Anal. Chim. Acta, 1982, 134, 13-19.

64. Whitten, W. B.; Ross, H. H. Anal. Chem., 1979, 51, 417-419.

65. Hieftje, G. M.; Travis, J. C.; Lytle, F. E. , Eds. "Lasers in Chemical Analysis," Humana: Clifton, NJ; 1981.

66. Yeung, E. S.; Sepaniak, M. J. Anal. Chem., 1980, 52, 1465A-1481A.

67. Stone, J. J. Opt. Soc. Am. , 1972, 62, 327-328.

68. Sepaniak, M. J.; Yeung, E. S. Anal. Chem., 1977, 49, 1554-1556.

69. Woodruff, S. D.; Yeung, E. S. Anal. Chem., 1982, 1174-1178.

70. Tong, W. G.; Yeung, E. S. Talanta, 1984, 31, 659-665.

71. Yeung, E. S.; Steenhoek, L. E.; Woodruff, S. D.; Kuo, J. C. Anal. Chem., 1980, 52, 1399-1402.

72. Harris, J. M.; Chrisman, R. W.; Lytle, F. E.; Tobias, R. A. Anal. Chem., 1976, 48, 1937-1943.

73. Diebold, G. J.; Zare, R. N. Science, 1977, 19, 1439-41.

74. Sepaniak, M. J.; Yeung, E. S. J. Chromatogr., 1980, 190, 377-383.

75. Hershberger, L. W.; Callis, J. B.; Christian, G. D. Anal. Chem., 1979, 51, 1444-1446.

76. Folestad, S.; Johnson, L.; Josefsson, G.; Galle, B. Anal. Chem., 1982, 54, 925-929.

77. Hill, D. W.; Powell, T. "Non-Dispersive Infra-Red Gas Analysis in Science, Medicine and Industry," Plenum: New York, NY; 1968.

78. Hu, C.; Whinnery, J. R. Appl. Opt. , 1973, 12, 72-79.

79. Jackson, W. B.; Amer, N. M.; Boccara, A. C.; Fournier, D. Appl. Opt. , 1981, 20, 1333-1344.

80. Long, M. E.; Swofford, R. L.; Albrecht, A. C. Science, 1976, 191, 183-184.

81. Collette, T. W.; Parekh, N. J.; Griffin, J. H.; Carreira, L. A.; Rogers, L. B. Appl. Spec. , 1986, 40, 164-169.

82. Dovichi, N.; Nolan, T. G.; Weimer, W. A. Anal. Chem., 1984, 56, 1700-1704.

83. Wylie, I. W.; Lai, E. P. C. Appl. Spec. , 1986, 40, 169-180.

84. Peck, K.; Fotiou, F. K.; Morris, M. D. Anal. Chem., 1985, 57, 1359-1362.

85. Harris, T. D. Anal. Chem., 1982, 54, 741A-745A.

86. Harris, J. M.; Dovichi, N. J. Anal. Chem., 1980, 52, 695A-706A.

87. Wilson, S. A.; Yeung, E. S. Anal. Chim. Acta, 1984, 157, 53-63.

88. Dovichi, N. J.; Harris, J. M. Anal. Chem., 1979, 51, 728-731.

89. Dovichi, N. J.; Harris, J. M. Anal. Chem., 1981, 53, 106-109.

90. Swofford, R. L.; Morrell, J. A. J. Appl. Phys., 1978, 49, 3667-3674.

91. Haushalter, J. P.; Morris, M. D. Appl. Spectrosc., 1980, 34, 445-447.

92. Mori, K.; Imasaka, T.; Ishibashi, N. Anal. Chem., 1983, 55, 1075-1079.

93. Fang, H. L.; Swofford, R. L. In "Ultrasensitive Laser Spectroscopy," Kliger, D. S. , Ed.; Academic Press: New York, 1983; 219-229.

94. Yang, Y. Anal. Chem., 1984, 56, 2336-2338.

95. Yang, Y.; Hairrell, R. E. Anal. Chem., 1984, 56, 3002-3004.

96. Pang, T. -K. J.; Morris, M. D. Anal. Chem., 1984, 56, 1467-1469.

97. Pang, T. -K. J.; Morris, M. D. Appl. Spectrosc., 1985, 39, 90-93.

98. Gordon, J. P.; Leite, R. C. C.; Moore, R. S.; Porto, S. P. S.; Whinney, J. R. J. Appl. Phys., 1965, 36, 3-8.

99. Carman, R. O.; Kelley, P. L. Appl. Phys. Lett., 1968, 12, 241-243.

100. Mho, S. I.; Yeung, E. S. Anal. Chem., 1985, 57, 2253-2256.

101. Wilson, S. A.; Yeung, E. S. Anal. Chem., 1985, 57, 2611-2614.

102. Synovec, R. E.; Yeung, E. S. Anal. Chem., 1985, 57, 2606-2610.

103 Bobbitt, D. R.; Yeung, E. S. Anal. Chem., 1984, 56, 1577-1581.

104. Ducloy, M.; Snyder, J. J. Proc. SPIE, 1983, 426, 87-90.

105. Sheldon, S. J.; Knight, L. V.; Throne, J. M. Appl. Opt., 1982, 21, 1663-1669.

106. Carter, C. A.; Harris, J. M. Appl. Opt., 1984, 23, 476-481.

107. Pang, T. -K. J.; Morris, M. D. Anal. Chem., 1985, 57, 2153-2155.

108. Crouthamel, C. E.; Diehl, H. Anal. Chem., 1948, 20, 515-520.

109. Noble, F. W.; Abel, K.; Cook, P. W. Anal. Chem., 1964, 36, 1421-1427.

110. Testerman, M. K.; McLeod, P. C. , in "Gas Chromatography," Brenner, N.; Cullen, J. E.; Weiss, M. D. , Eds.; Academic Press: New York, 1962; p. 183.

111. Grice, H. W.; David, D. J. J. Chromatogr. Sci., 1967, 7, 239-247.

112. David, D. J. "Gas Chromatographic Detectors," John Wiley and Sons: New York, 1974; pp. 144-164.

113. Todd, T.; DeBord, D. American Lab., Dec. 1970, 56-61.

114. Hartmann, C. H. Anal. Chem., 1971, 43, 113A-125A.

115. Synovec, R. E.; Yeung, E. S. Anal. Chem., 1983, 54, 1599-1603.

116. Synovec, R. E.; Yeung, E. S. J. Chromatogr., 1984, 283, 183-190.

117. Wilson, S. A.; Yeung, E. S. Anal. Chim. Acta, 1984, 157, 53-63.

118. Wilson, S. A.; Yeung, E. S.; Bobbitt, D. R. Anal. Chem.,1984, 56, 1457-1460.

119. Bobbitt, D. R.; Yeung, E. S. Anal. Chem., 1984, 56, 1577-1581.

120. Bevan, S. C.; Gough, T. A.; Thorburn, S. J. Chromatogr., 1969, 42,

336-348.

121. Martin, A. J. P.; James, A. T. Biochem. J., 1956, 63, 138-143.

122. Nerheim, A. G. J. Chromatogr. Sci., 1977, 15, 465-468.

123. Guillemin, C. L.; Auricourt, M. F. J. Gas Chromatogr., 1963, 1, 24-29.

124. Nerheim, A. G. Anal. Chem., 1963, 35, 1640-1644.

125. Walsh, J. T.; Rosie, D. M. J. Gas Chromatogr., 1967, 5, 223-240.

126. Kiran, E.; Gillham, J. K. Anal. Chem., 1975, 47, 983-995.

127. Lloyd, R. J.; Henderson, D. E.; Uden, P. C. Anal. Chem., 1976, 48, 1645-1646.

128. Lanser, A. C.; Ernst, J. O.; Kwolek, W. F.; Dutton, H. J. Anal. Chem., 1973, 45, 2344-2348.

129. Bevan, S. C.; Gough, T. A.; Thorburn, S. J. Chromatogr., 1969, 44, 14-24.

ACKNOWLEDGEMENTS

For his thoughtful direction of my graduate research I would like to thank Dr. Edward S. Yeung. I would also like to acknowledge Dr. Dennis Johnson for his support and encouragement as well as his excellent teaching.

All the members of Dr. Yeung's group were fine friends and colleagues. Anna Yeung and her family provided a friendly base for the group. I wish all those I worked with the best of luck. This also goes for Zhu, even though he gave me "no cooperation."

For their friendship and fellowship I will always be indebted to Barb, Patrice and Cecilia. In Don, Susan, Joel and Barbara, who opened homes and lives to me, I found more good friends.

I would like to tell my family in Colorado and Minnesota how much I love them and appreciate their support.

Finally, to my love Rob, who shares so much with me, I thank you for making graduate school a true adventure.